STATISTICAL INFERENCE FOR MANIFOLD SIMILARITY AND ALIGNABILITY ACROSS NOISY HIGH-DIMENSIONAL DATASETS

BY HONGRUI CHEN[1] AND RONG MA[2,3,4,a]

[1]*Weiyang College, Tsinghua University*

[2]*Department of Biostatistics, Harvard T.H. Chan School of Public Health*

[3]*Department of Data Science, Dana-Farber Cancer Institute*

[4]*Eric and Wendy Schmit Center, Broad Institute*
[a]*rongma@hsph.harvard.edu*

The rapid growth of high-dimensional datasets across various scientific domains has created a pressing need for new statistical methods to compare distributions supported on their underlying structures. Assessing similarity between datasets whose samples lie on low-dimensional manifolds requires robust techniques capable of separating meaningful signal from noise. We propose a principled framework for statistical inference of similarity and alignment between distributions supported on manifolds underlying high-dimensional datasets in the presence of heterogeneous noise. The key idea is to link the low-rank structure of observed data matrices to their underlying manifold geometry. By analyzing the spectrum of the sample covariance under a manifold signal-plus-noise model, we develop a scale-invariant distance measure between datasets based on their principal variance structures. We further introduce a consistent estimator for this distance and a statistical test for manifold alignability, and establish their asymptotic properties using random matrix theory. The proposed framework accommodates heterogeneous noise across datasets and offers an efficient, theoretically grounded approach for comparing high-dimensional datasets with low-dimensional manifold structures. Through extensive simulations and analyses of multi-sample single-cell datasets, we demonstrate that our method achieves superior robustness and statistical power compared with existing approaches.

1. Introduction. Recent advances in data collection and computation have made large, high-dimensional datasets increasingly available across domains such as astronomy, business analytics, human genetics, and microbiology. Despite their high ambient dimensionality, the underlying signal structure of many datasets can often be effectively represented by some ideal low-dimensional structure, such as a smooth manifold. This "manifold hypothesis" [21] forms the foundation of important fields of data science, such as manifold learning [33], domain adaptation [31] and representation learning [6]. When analyzing multiple datasets that may differ in their underlying structures, it is often essential to characterize and quantify the similarity between the distributions of their low-dimensional representations on manifolds. Such analysis enables assessment of the diversity of information contained in these datasets and the extent to which their underlying signals overlap, offering an integrated perspective that reveals high-level relationships among datasets that are not apparent when each dataset is analyzed in isolation.

A closely related problem is testing whether two datasets originate from the same latent structure, which calls for broadly applicable and robust two-sample testing methods. Classical parametric tests such as Hotelling's T^2 and Student's t were devised for low-dimensional

data. Under nonparametric setup, many widely used statistical procedures for comparing two datasets were likewise developed under the finite dimensional setting, such as energy distance tests [14, 37], kernel maximum mean discrepancy tests [2, 22, 23], graph-based tests [11, 12], Wasserstein distance tests and their projected variants [41], and interpoint distance tests [5, 27, 38, 40]. Although these procedures are provably consistent in their classical regimes, their calibration and statistical power often deteriorate as the data dimensionality increases. Moreover, most nonparametric approaches focus on comparing the entire ambient-space distributions underlying each dataset. This panoramic perspective offers flexibility but can be restrictive in practice because accurately estimating high-dimensional distributions from finite samples is intrinsically difficult. This challenge gives rise to several limitations in existing methods. For instance, the performance of MMD is highly sensitive to bandwidth selection [2, 22, 23]; the unprojected Wasserstein distance suffers from slow finite-sample convergence; projected Wasserstein methods are sensitive to hyperparameter choices (such as kernel type, regularization, and projection dimension), rely on nonconvex optimization without global optimality guarantees, and are computationally expensive [41]; and edge-count graph-based tests may lose power under scale alternatives or become unstable when sample sizes are unbalanced [11, 12].

For comparing noisy high-dimensional datasets, a more robust alternative approach is to compare *structural properties* of their underlying distributions, such as feature covariance. In this connection, a prominent line of work focuses on testing large-scale multiple hypotheses about the entry-wise equality of the sparse population covariance or precision matrices between two datasets [9, 30, 44, 45]. When the data matrices appear to exhibit low-rank structures, another group of work focuses on inference on the leading eigenvalues or eigensubspaces of the population covariance matrices [3, 18, 32, 34, 36, 46], distance covariance matrices [28], or canonical correlation matrices [4, 47], which can be used to detect structural similarity or differences between two high-dimensional datasets. Despite their conceptual simplicity and efficacy in comparing high-dimensional datasets, none of these methods seems to have fully incorporated the manifold hypothesis into their design principles, particularly in leveraging the smoothness of the underlying low-dimensional signals to enhance the power of the inference procedure. More importantly, most existing approaches assume homogeneous noise both within and across datasets, making them vulnerable to inferential bias or even inconsistency when applied to heterogeneous data characterized by complex, heteroskedastic noise structures.

To address these limitations, in this work we consider a general manifold signal-plus-noise matrix model and propose a unified statistical framework, Manifold Spectrometrics (MS), for inferring similarity and alignability between high-dimensional datasets with respect to their latent low-dimensional signal structures. Our approach differs from existing eigenstructure inference methods in three key aspects: (i) it builds on the *manifold hypothesis* to enable designing novel statistical procedures with enhanced power for inference on datasets with low-dimensional smooth manifold structures; (ii) it leverages recent advances in random matrix theory to estimate and correct for the effects of *heteroskedastic noise* across datasets, thereby enabling more robust inference under data heterogeneity; and (iii) it introduces a quantitative *distance measure* between datasets based on their population-level signal profiles represented by the latent manifolds, offering a more interpretable characterization of similarity than the binary outcomes produced by traditional hypothesis testing procedures.

Suppose we observe two data matrices Y_1 and Y_2, generated from the manifold signal-plus-noise matrix model:

$$(1) \qquad Y_k = S_{\mathrm{samp},k} + \Sigma_k^{1/2} X_k \in \mathbb{R}^{p \times N_k}, \quad k = 1, 2$$

where $S_{\mathrm{samp},k} = [S_{1,k}, \ldots, S_{N_k,k}]$ collects N_k noiseless samples (or signals) drawn from a low-dimensional smooth manifold $\mathcal{M}_k$ embedded in $\mathbb{R}^p$ (see Section 2.2 for a more formal

description), $\Sigma_k \in \mathbb{R}^{p \times p}$ is a deterministic matrix encoding the noise covariance, and $X_k = [x_{i\mu,k}] \in \mathbb{R}^{p \times N_k}$ has independent entries with mean zero and unit variance. For the ambient space dimensionality p, we will consider the high-dimensional regime where $p, N_k \to \infty$ with $p/N_k \to \varphi_k$. This model generalizes the classical matrix denoising model and the homoskedastic noisy manifold model in the existing literature [15, 19, 29]. In addition, we assume the data is already centered and define the sample covariance $Q_k := Y_k Y_k^\top / N_k$, whose population counterpart is $\widetilde{\Sigma}_k := \mathbb{E}[Q_k] = \Sigma_k + M_k$, where $M_k := \frac{1}{N_k} \mathbb{E}[S_{\mathrm{samp},k} S_{\mathrm{samp},k}^\top]$. Under this model, our goal is to make statistical inferences about the similarity and alignability of the latent manifold structures underlying Y_1 and Y_2. Specifically, by manifold similarity inference, we refer to defining a distance measure between distributions supported on latent manifold structures and developing an accurate estimator of this measure along with its uncertainty quantification. By manifold alignability inference, we refer to constructing a rigorous statistical test to evaluate whether the distributions on the latent manifolds of two datasets are geometrically equivalent.

Our key innovation lies in establishing a theoretical connection between the manifold geometry of $\mathcal{M}_k$, which represents the population-level structure, and the spectral properties of $\widetilde{\Sigma}_k$, Σ_k, and M_k, which are derived from finite-sample observations. This linkage enables the formulation of a natural distance measure between noisy, high-dimensional datasets based on their latent population signatures, effectively capturing discrepancies between their underlying low-dimensional manifold structures. Moreover, it allows the smooth, low-dimensional geometry to be leveraged for more effective separation of signal from heteroskedastic noise in both datasets. By bridging population-level geometric properties with finite-sample spectral behavior, this framework provides a foundation for developing consistent inference procedures for manifold learning grounded in random matrix theory.

Our main methodological contributions are:

- We introduce the normalized Manifold Spectral Distance (nMSD), a scale-invariant metric that quantifies the difference between the population-level low-dimensional signal structures of two datasets. We further propose a computationally efficient estimator of the nMSD based on noisy observations under heterogeneous noise and unequal sample sizes, and establish its consistency and asymptotic normality in high-dimensional settings, thereby providing theoretical justification for manifold similarity inference.
- We formulate the manifold alignability problem as a global two-sample hypothesis test on the equivalence of latent manifold structures with respect to the nMSD metric. A corresponding statistical test is proposed, and its asymptotic validity and power consistency are established under high-dimensional asymptotic settings.
- As a key component of our inferential framework, we develop entrywise consistent estimators for data-specific, piecewise-diagonal noise covariance matrices, enabling accurately accounting for the effects arising from heteroskedastic noise. Our approach integrates the low-rank truncation technique with a one-dimensional Potts segmentation method, which can be efficiently solved using dynamic programming.
- We extend the concept of nMSD to general nonlinear settings using kernel-based manifold learning. We propose estimators of the kernelized nMSD and establish their consistency in high-dimensional regimes, enabling more flexible comparison of datasets via their spectral embeddings in reproducing kernel Hilbert spaces (RKHS) rather than in the ambient Euclidean space.

To support these methodological advances, we develop novel theoretical tools that are broadly applicable beyond the present context. In particular, our derivation of asymptotic normality results relies on key delocalization properties of the signal spectral representations, established by exploiting the latent manifold geometry. Moreover, our inference procedures are

constructed through a careful analysis of a system of secular equations under heteroskedastic noise. Further details are provided in Sections 2.4, 4.1, and 4.2.

The paper is organized as follows. We first conclude this section by collecting the main notation used throughout the paper. In Section 2 we formally introduce our data-generating model and the manifold spectral distance, and characterize the connection between manifold geometry and the matrix spectral properties. Section 3 presents our proposed methods and their asymptotic properties. In Section 4 we outline our derivation of the main theoretical results and discuss some technical innovations of interest. In Section 5 we conduct extensive simulations and analyze a real-world biological data to assess the empirical performance of proposed methods.

We use $\odot$ for elementwise Hadamard products: for equal-shaped arrays A, B, $(A \odot B)_{ij} = A_{ij}B_{ij}$, and $A^{\odot 2}$ denotes the elementwise square. The symbol $\otimes$ denotes the Kronecker product; for vectors it reduces to the outer (tensor) product, and $u^{\otimes 4} := u \otimes u \otimes u \otimes u$. $\mathrm{Cum}_4(S)$ denotes the fourth-order cumulant tensor of a random vector S, with entries $\mathrm{Cum}(S_{i_1}, S_{i_2}, S_{i_3}, S_{i_4})$. For stochastic orders, $X_N = O_{\mathbb{P}}(a_N)$ means X_N/a_N is bounded in probability, and $X_N = o_{\mathbb{P}}(a_N)$ means $X_N/a_N \to 0$ in probability. For a sequence of events (E_N), we say that E_N holds *with high probability* (w.h.p.) if there exist constants $C, c > 0$, independent of N, such that

$$\mathbb{P}(E_N) \geq 1 - CN^{-c}$$

for all sufficiently large N. Matrix norms: $\|A\|_{\mathrm{F}} = \sqrt{\sum_{i,j} A_{ij}^2}$ (Frobenius) and $\|A\|_{\mathrm{op}} = \sup_{\|x\|_2=1} \|Ax\|_2$. And $\|\cdot\|_{\psi_2}$ denotes the sub-Gaussian (Orlicz) norm: $\|X\|_{\psi_2} := \inf\{t > 0 : \mathbb{E}\exp(X^2/t^2) \leq 2\}$. For any bounded linear operator $T : \mathcal{H} \to \mathcal{H}$, write $[T]$ for its matrix in a fixed orthonormal basis $(e_1, \ldots, e_p)$. Likewise, for $A : \mathcal{H} \to \mathbb{R}^N$, let $[A] \in \mathbb{R}^{N \times p}$ be the matrix of A in the fixed basis of $\mathcal{H}$ and the standard basis of $\mathbb{R}^N$. Throughout the paper, $X_n \xrightarrow{\mathbb{P}} X$ denotes convergence in probability, and $X_n \xrightarrow{d} X$ denotes convergence in distribution. We also denote by $\mathbb{O}(p)$ the orthogonal group in dimension p, $\mathbb{O}(p) := \{Q \in \mathbb{R}^{p \times p} : Q^\top Q = I_p\}$.

2. Noisy Manifold Model, Spectral Distance, and Matrix Spectral Properties. In this section, we formally introduce the manifold signal-plus-noise model and explain how the noiseless signals arise from the underlying manifold structure. We then present a rigorous definition of the manifold spectral distance between two distributions on manifolds and describe the key spectral properties of the data matrices induced by the manifold geometry.

2.1. *Signal-plus-noise matrix model.* For the noisy observations, we assume that each data matrix Y_k for $k = 1, 2$ follows the signal-plus-noise model defined in (1). Without loss of generality, we assume the data is already centered so that $\mathbb{E}[Y_k] = \mathbb{E}[S_{\mathrm{samp},k}] = 0$.

We also make the following assumptions about the noise component $\Sigma_k^{1/2}X_k$ and the dimensionality of Y_k. For notational simplicity, throughout, we drop the dataset index k whenever it is clear from the context that the statement applies to both datasets, and reinstate the subscript only when it is necessary to distinguish between them.

ASSUMPTION 2.1 (High-dimensional regime and block-heteroskedastic noise). Throughout, we assume the following conditions hold.

(i) **Proportional high-dimensional regime.** For each dataset, let $p, N \to \infty$ with $p/N \to \varphi \in (0, \infty)$.
(ii) **Entrywise scaling and sub-Gaussian tails.** The entries $x_{i\mu}$ are independent across (i, μ), satisfy $\mathbb{E}x_{i\mu} = 0$ and $\mathrm{Var}(x_{i\mu}) = 1$, and are uniformly sub-Gaussian: there exists a constant $K < \infty$ such that $\|x_{i\mu}\|_{\psi_2} \leq K$ for all i, μ.

(iii) **Zero third cumulant.** The noise is symmetric with vanishing third cumulant $\kappa_3 = 0$, that is, $\mathbb{E}x_{i\mu}^3 = 0$ for all i and μ.

(iv) **Diagonal block-heteroskedastic noise.** The noise covariance is diagonal and piecewise constant along a fixed feature order: there exists a partition of $\{1,\ldots,p\}$ into consecutive blocks $I_1,\ldots,I_{K_p}$ such that $\Sigma = \mathrm{diag}(\sigma_1,\ldots,\sigma_p)$, where $\sigma_i = \tau_j$ for all $i \in I_j$, with noise levels uniformly bounded: $0 < \sigma_{\min} \le \tau_j \le \sigma_{\max} < \infty$ for all j. Moreover, the number of blocks K_p may depend on p, but satisfies $K_p = o(p)$, and the minimal block length diverges $m_p := \min_{1 \le j \le K_p} |I_j| \to \infty$ as $p \to \infty$.

Conditions (i) (ii) and (iii) are standard in random matrix theory and facilitate precise asymptotic analysis of the matrix spectrum [1, 20]. Condition (iv) allows for heteroskedasticity in the noise components, representing a substantially weaker assumption than the commonly imposed homoskedastic or isotropic noise conditions in the existing literature [15, 16, 19]. The block-structured constraint on noise variance is motivated by a wide range of biomedical applications. In single-cell analysis, for example, the variances of gene expression across cell populations often exhibit group structures that reflect distinct genetic programs comprising functionally related genes. Genes within the same program tend to share similar variance profiles, whereas those belonging to different programs display distinct patterns; see Section E.2 in supplement for empirical evidence supporting this block-structured variance pattern in real biological data.

This structural assumption facilitates efficient estimation and separation of the noise and signal components. Without such structure, for example, when Σ were an arbitrary unknown diagonal matrix, it would be difficult, if not impossible, to disentangle the noise from the low-rank signal, resulting in spectral estimates that conflate the true signal with noise anisotropy.

2.2. *Latent manifold model for noiseless samples.* For the latent signal component $S_{\mathrm{samp},k} = [S_{1,k},\ldots,S_{N_k,k}]$ in the noisy observation model (1), we assume the noiseless samples $\{S_{i,k}\}_{1 \le i \le N_k}$ are independently drawn from a distribution supported on a low-dimensional smooth manifold that is embedded into the ambient high-dimensional space $\mathbb{R}^p$. A rigorous formulation of this assumption is provided below, which generalizes the setup commonly adopted in the manifold learning literature [15–17, 43].

ASSUMPTION 2.2 (Manifold model for signals). For $k \in \{1,2\}$, let $(\mathcal{M}_k, g_k)$ be a connected, compact, m_k-dimensional Riemannian manifold and let $\iota_k : \mathcal{M}_k \to \mathbb{R}^p$ be an isometric embedding satisfying $\dim(\iota_k(\mathcal{M}_k)) = n_k \le p$. Let $\mathcal{B}(\mathcal{M}_k)$ denote the Borel σ–algebra on $\mathcal{M}_k$, and let $\mathbb{P}_k$ be a probability measure on $(\mathcal{M}_k, \mathcal{B}(\mathcal{M}_k))$. Assume $\mathbb{P}_k$ is absolutely continuous with respect to the Riemannian volume measure vol_{g_k} on $\mathcal{M}_k$, with density bounded and bounded away from zero, that is, $0 < c_{k,\min} \le \frac{d\mathbb{P}_k}{d\mathrm{vol}_{g_k}}(x) \le c_{k,\max} < \infty$ for all $x \in \mathcal{M}_k$. Let $\widetilde{\mathcal{F}}_k$ be the Borel σ–algebra on $\iota_k(\mathcal{M}_k)$, and define the pushforward measure on $(\iota_k(\mathcal{M}_k), \widetilde{\mathcal{F}}_k)$ by $\rho_k := \mathbb{P}_k \circ \iota_k^{-1}$. For the noiseless samples, we assume that $S_{1,k},\ldots,S_{N_k,k} \overset{\mathrm{i.i.d.}}{\sim} \rho_k$, which are supported on $\iota_k(\mathcal{M}_k)$.

Under Assumption 2.2, since $n := \dim(\iota(\mathcal{M})) \le p$, there exists an orthonormal matrix $R \in \mathbb{O}(p)$ such that $(R \circ \iota)(\mathcal{M}) \subset \mathbb{R}^n \times \{0\}^{p-n}$. Define the coordinate functions

$$(2) \qquad f_j(x) := e_j^\top (R \circ \iota)(x), \qquad j = 1,\ldots,n, \ \ x \in \mathcal{M}.$$

Then for every $x \in \mathcal{M}$, we can write

$$(3) \qquad (R \circ \iota)(x) = \big(f_1(x),\ldots,f_n(x),0,\ldots,0\big) \in \mathbb{R}^p,$$

for the noiseless samples $S_i \sim \rho$ supported on $\iota(\mathcal{M})$, we have

(4) $$RS_i = \big(f_1(S_i), \ldots, f_n(S_i), 0, \ldots, 0\big), \qquad i = 1, \ldots, N.$$

Assumption 2.2 is motivated by real-world applications (for example, see applications in single-cell analysis in Section 5.2), where the objects of interest are the signal structures represented by the embedded manifold $\iota(\mathcal{M})$ and the pushforward probability measure ρ, rather than the latent manifold $\mathcal{M}$ and the probability measure $\mathbb{P}$. The existence of the isometric embedding ι and orthogonal matrix R that yields a sparse Euclidean representation (3) of the manifold follows from the fundamental insights in manifold embedding theory. For example, the Nash embedding theorem ensures the existence of $n \leq m(3m+11)/2$ when $\mathcal{M}$ is a compact Riemannian manifold, and of $n \leq m(m+1)(3m+11)/2$ when $\mathcal{M}$ is a non-compact Riemannian manifold; see, for example, Theorem E.2 of [16] for details. This insight has been utilized for theoretical analysis in prior work [15, 16].

Under Assumption 2.2, the reduction in (4) implies that the noiseless samples are effectively supported on a n-dimensional subspace. This characterization enables the inference and comparison of latent signal structures across datasets in a basis-independent manner, as will be demonstrated below. We next introduce the population and empirical covariance matrices associated with the latent manifold model.

DEFINITION 2.1 (Population and empirical signal covariance matrices). Let $S_1, \ldots, S_N \in \mathbb{R}^p$ be centered noiseless samples drawn i.i.d. from ρ supported on $\iota(\mathcal{M})$ as in Assumption 2.2. Denote $S_{\mathrm{samp}} = [\, S_1, \ldots, S_N \,] \in \mathbb{R}^{p \times N}$. Then the population and empirical signal covariance matrices are defined as

(5) $$M := M(\rho) = \mathbb{E}[S_i S_i^\top] = \int_{\iota(\mathcal{M})} S_i S_i^\top \, d\rho \in \mathbb{R}^{p \times p}, \qquad \widehat{M} := \frac{1}{N} S_{\mathrm{samp}} S_{\mathrm{samp}}^\top \in \mathbb{R}^{p \times p}.$$

The population covariance matrix M is uniquely determined by $\rho := \mathbb{P} \circ \iota^{-1}$, the pushforward probability measure supported on $\iota(\mathcal{M}) \subset \mathbb{R}^p$ associated with $(\mathcal{M}, \mathbb{P}, \iota)$. Because $\iota(\mathcal{M})$ is compact and the samples are centered, $M = \mathbb{E}[S_i S_i^\top]$ exists, has $\mathrm{rank}(M) \leq n$, and as a linear operator on $\mathbb{R}^p$ vanishes on $V^\perp$ where $V := \mathrm{span}(\iota(\mathcal{M}))$. For any unit vector $v \in \mathbb{R}^p$,

$$v^\top M v = \mathrm{Var}\big(\langle v, S_i \rangle\big) := \int_{\iota(\mathcal{M})} \langle v, S_i \rangle^2 d\rho,$$

is the variance of ρ along direction v. Hence the top eigenvalue of the population covariance matrix M, given by

$$\mathcal{D}_1 = \sup_{\|v\|_2 = 1} v^\top M v,$$

characterizes the principal variance of the distribution ρ on the embedded manifold $\iota(\mathcal{M})$ along the axis of maximal spread. Recursively, the k-th eigenvalue $\mathcal{D}_k$ arises from the same maximization subject to additional constraint $v \perp \mathrm{span}\{\eta_1, \ldots, \eta_{k-1}\}$; directions orthogonal to V carry zero variance. From the above discussion, we can see that $\{\mathcal{D}_k\}_{1 \leq k \leq n}$ capture the overall magnitude of the latent signal structure along its intrinsic principal axes. Following the the convention in [15, 18, 29, 32], hereafter, we refer to these population-level eigenvalues $\{\mathcal{D}_k\}_{1 \leq k \leq n}$ as the true signal strength parameters. These parameters play a key role in our subsequent development of manifold spectral distance metric.

Importantly, these spectral parameters are orthogonally invariant to the choice of basis coordinate in $\iota(\mathcal{M})$, and are intrinsic to the ambient Euclidean space $\mathbb{R}^p$. Specifically, for any orthogonal transformation $R \in \mathbb{O}(p)$, we have

$$M^{(\mathrm{rot})} = \mathbb{E}[(RS_i)(RS_i)^\top] = R M R^\top, \qquad \widehat{M}^{(\mathrm{rot})} = \frac{1}{N}(RS_{\mathrm{samp}})(RS_{\mathrm{samp}})^\top = R \widehat{M} R^\top.$$

Since orthogonal changes of coordinates act by congruence ($M \mapsto RMR^\top$), the eigenvalues remain invariant under changes of basis, while the eigenspaces are preserved up to rotation.

2.3. *Manifold spectral distance.* To enable comparison of the underlying manifold structures across datasets, we next introduce a robust, scale-invariant distance measure based on the eigenvalues $\{\mathcal{D}_k\}_{1 \leq k \leq n}$ of the population covariance matrix.

DEFINITION 2.2 (Normalized population principal variances). Let ρ be the pushforward measure defined in Assumption 2.2, and $\mathcal{D}_1 \geq \mathcal{D}_2 \geq \cdots$ be the ordered eigenvalues of M associated with ρ. If we denote $\mathcal{D}^{(r)} := (\mathcal{D}_1, \ldots, \mathcal{D}_r)^\top$ containing the leading r eigenvalues with $r \leq p$, then the normalized top-r principal variances vector of ρ is defined as

$$\Pi_r(\rho) := \frac{\mathcal{D}^{(r)}}{\mathbf{1}^\top \mathcal{D}^{(r)}} \in \Delta^{r-1} := \Big\{ x \in \mathbb{R}^r : x_k \geq 0, \ \sum_{k=1}^r x_k = 1 \Big\}.$$

DEFINITION 2.3 (Manifold spectral distance). Let ρ_k be a probability measure defined by Assumption 2.2, associated with some $(\mathcal{M}_k, \mathbb{P}_k, \iota_k)$ for $k = 1, 2$. Let $\Pi_r(\rho_k)$ be the normalized top-r principal variances of ρ_k. The normalized manifold spectral distance (nMSD) between ρ_1 and ρ_2 is defined as $d_r(\rho_1, \rho_2) := \big\| \Pi_r(\rho_1) - \Pi_r(\rho_2) \big\|_2$.

Compared with existing approaches that quantify dataset similarity using distance measures on entire distributions, such as KL divergence or MMD, or on covariance matrices, such as the Frobenius distance, the proposed manifold spectral distance offers two key advantages. First, it is inherently invariant to scale changes and orthogonal transformations of the data. Second, it is robust to minor geometric or distributional shifts that do not affect the leading principal variances, thereby capturing more stable and intrinsic structural relationships between datasets.

REMARK 2.4 (Choosing the working rank r). If the two manifolds share a known intrinsic dimension n, one can naturally set $r = n$. More generally, if their intrinsic dimensions are n_1 and n_2, it is reasonable to take $r = \max\{n_1, n_2\}$. In practice, when n or (n_1, n_2) are unknown, one may estimate the signal rank using existing methods like [25] and [10]. Accordingly, we treat $r = n$ as given in what follows; for two datasets we set $r = \max\{\hat{r}_1, \hat{r}_2\}$.

Notably, our distance measure is defined on the pushforward distributions ρ_1 and ρ_2, rather than solely on their support manifolds $\iota_1(\mathcal{M}_1)$ and $\iota_2(\mathcal{M}_2)$. In particular, two datasets may reside on the same embedded manifold, i.e., $\iota_1(\mathcal{M}_1) = \iota_2(\mathcal{M}_2)$, yet differ in their sampling densities, thereby inducing distinct population covariance matrices M_1 and M_2, as well as different normalized principal variances $\Pi_r(\rho_1)$ and $\Pi_r(\rho_2)$. In this sense, d_r is designed to capture both geometric discrepancies between the latent manifolds and differences in their underlying sampling distributions. Indexing by ρ emphasizes that our comparison operates at the level of *distributions supported on embedded manifolds*, rather than on the manifolds alone. In Section A of the Supplement, we provide two examples demonstrating some basic properties of $d_r(\rho_1, \rho_2)$.

2.4. *Spectral properties of the signal matrices.* When the noiseless samples $S_1, \ldots, S_N$ are *i.i.d.* sampled from the above latent manifold model, the corresponding signal matrix S_{samp} and the underlying population covariance matrix M exhibit several important spectral properties. These properties, summarized below, play a key role in our method development.

PROPOSITION 2.5 (PCA alignment within the signal subspace). *Under Assumption 2.2, let $S \in \mathbb{R}^p$ be centered with $\mathbb{E}[S] = 0$ and let $M := \mathbb{E}[SS^\top]$. With the coordinate functions $f_1, \ldots, f_n$ already defined by $(R \circ \iota)(x) = (f_1(x), \ldots, f_n(x), 0, \ldots, 0)$, we may, without loss of generality, apply an additional orthogonal change of coordinates within the first n axes so that for the same notation $f_1, \ldots, f_n$, we have $\mathbb{E}[f_i(S)] = 0$, $\mathbb{E}[f_i(S) f_j(S)] = 0$ $(i \neq j)$, and $\mathcal{D}_i = \mathbb{E}[f_i(S)^2]$, with $\mathcal{D}_1 \geq \cdots \geq \mathcal{D}_n \geq 0$. In particular, $\{\mathcal{D}_i\}_{i=1}^n$ are exactly the nonzero eigenvalues of M.*

Let $S_{\mathrm{samp}} = U_{\mathrm{samp}} D_{\mathrm{samp}} V_{\mathrm{samp}}^\top$ be the SVD of S_{samp}. For any $R \in \mathbb{O}(p)$, a change of ambient basis gives $S_{\mathrm{samp}}^{(\mathrm{rot})} = R\, S_{\mathrm{samp}} = (R\, U_{\mathrm{samp}})\, D_{\mathrm{samp}}\, V_{\mathrm{samp}}^\top$. Hence the singular values D_{samp} and the right singular vectors V_{samp} are invariant under ambient orthogonal rotations; only the left singular vectors rotate.

PROPOSITION 2.6 (Low-rankness of the sample signal matrix). *Under Assumption 2.2, let $S_{\mathrm{samp}} = [S_1, \ldots, S_N] \in \mathbb{R}^{p \times N}$. Then $\mathrm{rank}(S_{\mathrm{samp}}) \leq n$. Moreover, if $N \geq n$, then $\mathrm{rank}(S_{\mathrm{samp}}) = n$ almost surely.*

Proposition 2.6 is intuitive since the noiseless samples are generated from a manifold embedded in a low-dimensional subspace. Even though the feature dimension p increases with the sample size N, the true signal dimension n and the rank of S_{samp} remain small.

PROPOSITION 2.7 (Matrix spectral concentration, stability, and delocalization). *Under Assumption 2.2, let $S_1, \ldots, S_N \in \mathbb{R}^p$ be centered noiseless samples drawn i.i.d. from ρ supported on $\iota(\mathcal{M})$. Let $(\mathcal{D}_k, \eta_k)_{k=1}^n$ be the nonzero eigenpairs of M with $\mathcal{D}_1 \geq \cdots \geq \mathcal{D}_n > 0$ and assume the uniform eigengap*

$$\inf_{1 \leq k \leq n} \min\{\mathcal{D}_{k-1} - \mathcal{D}_k,\ \mathcal{D}_k - \mathcal{D}_{k+1}\} > 0, \quad (\mathcal{D}_0 := +\infty,\ \mathcal{D}_{n+1} := 0).$$

Since $\iota(\mathcal{M})$ is compact, set $\kappa^2 := \sup_{x \in \iota(\mathcal{M})} \|x\|_2^2 < \infty$. Take the thin SVD $S_{\mathrm{samp}} = U_{\mathrm{samp}} D_{\mathrm{samp}} V_{\mathrm{samp}}^\top$ with $U_{\mathrm{samp}} \in \mathbb{R}^{p \times n}$, $V_{\mathrm{samp}} \in \mathbb{R}^{N \times n}$ containing orthonormal columns and $D_{\mathrm{samp}} = \mathrm{diag}(d_1, \ldots, d_n)$. Then for any $\delta \in (0,1)$, the following hold.

(i) ***Operator-norm concentration.*** *With probability at least $1 - \delta$,*

$$\left\| \widehat{M} - M \right\|_{\mathrm{op}} \leq \frac{4\kappa^2 \log(2/\delta)}{\sqrt{N}}.$$

(ii) ***Singular values and the spectrum of $\widehat{M}$.*** *The nonzero eigenvalues of $\widehat{M}$ are $\{d_i^2/N\}_{i=1}^n$. Moreover, for any fixed $\varepsilon > 0$, there exist constants $C, c > 0$ such that*

$$\Pr\left(\max_{1 \leq i \leq n} \left| d_i - \sqrt{N \mathcal{D}_i} \right| > \varepsilon \right) \leq C N^{-c}.$$

(iii) ***Coordinate-wise PCA approximation of right singular vectors.*** *For any fixed $i \in [n]$ and $\varepsilon > 0$, there exist $C, c > 0$ such that*

$$\Pr\left(\max_{1 \leq j \leq N} \left| V_{\mathrm{samp}}(j, i) - \frac{f_i(S_j)}{\sqrt{N \mathcal{D}_i}} \right| > \varepsilon \right) \leq C N^{-c}.$$

(iv) ***Delocalization of right singular vectors.*** *There exist $C, c > 0$ such that, with probability at least $1 - N^{-c}$,*

$$\forall\, 1 \leq i \leq n: \qquad \max_{1 \leq j \leq N} |V_{\mathrm{samp}}(j, i)| \leq \frac{C\sqrt{\log N}}{\sqrt{N}}.$$

Proposition 2.7 characterizes the asymptotic relationship between the singular values and vectors of the signal sample matrix S_{samp} and the underlying population ρ on the manifold. In particular, part (i) establishes the asymptotic equivalence between the population and the empirical covariance matrices; part (ii) connects the singular values of the signal matrix S_{samp} to the eigenvalues of the population covariance matrix M; part (iii) relates the right singular vectors, or the sample spectral embeddings, with the latent Euclidean representation of the noiseless samples on the manifold, providing a geometric interpretation of the singular vectors; and part (iv) describes a key delocalization property of the right singular vectors, which arises naturally from the smoothness of the latent manifold.

3. Main results. Building on the above results about the manifold signal-plus-noise model, we introduce a unified statistical framework for inferring the nMSD between two noisy high-dimensional datasets. The proposed method proceeds in two stages: first, we construct a consistent estimator of the unknown noise covariance matrix Σ (Section 3.1); second, we use this estimator to account for the noise heteroskedasticity and develop an estimator and associated inference procedures for the true nMSD (Sections 3.2 and 3.3).

3.1. *Noise variance estimation.* Leveraging the facts that the signal matrix S_{samp} is low-rank (Proposition 2.6) with delocalized singular vectors (Proposition 2.7), and that the noise covariance admits a block structure (Assumption 2.1), we propose computationally efficient noise estimators for each dataset. Specifically, our approach performs a low-rank fitting followed by one-dimensional Potts segmentation, which is solved exactly using dynamic programming [24, 42]. The details of the estimation procedure is summarized in Algorithm 1.

Algorithm 1: Noise variance estimation

Inputs: data matrix $Y \in \mathbb{R}^{p \times N}$; working rank $r = n \geq 1$; a fixed 1-D feature order on $\{1, \ldots, p\}$; segmentation penalty $\beta > 0$.

Output: $\widehat{\Sigma} = \mathrm{diag}(\widehat{\sigma}^{\mathrm{pwc}})$.

1. Low-rank fitting. Compute $Q = \frac{1}{N} Y Y^\top$. Obtain the best rank-n approximation $\widehat{C}_n = \widehat{U}_n \widehat{D}_n \widehat{U}_n^\top$ to Q via truncated SVD, where $\widehat{U}_n \in \mathbb{R}^{p \times n}$ and $\widehat{D}_n \in \mathbb{R}^{n \times n}$ contain leading n eigenvectors and eigenvalues of Q. Set the raw variance estimators as the spectral truncation residual diagonal $\widehat{\sigma} \leftarrow \mathrm{diag}(Q - \widehat{C}_n)$.

2. Piecewise smoothing via Potts segmentation. Regularize along the feature order by solving the Potts segmentation problem

$$(6) \qquad \widehat{\sigma}^{\mathrm{pwc}} \in \arg\min_{\sigma \in \mathbb{R}^p} \left\{ \sum_{i=1}^{p} (\widehat{\sigma}_i - \sigma_i)^2 + \beta \, \#\{1 \leq i < p : \sigma_{i+1} \neq \sigma_i\} \right\},$$

where β is a tuning parameter. This Potts segmentation problem is computed exactly by dynamic programming.

3. Return the noise covariance estimator. Set $\widehat{\Sigma} \leftarrow \mathrm{diag}(\widehat{\sigma}^{\mathrm{pwc}})$.

The diagonal, piecewise-constant structure of the noise covariance enables entrywise consistent estimation from the noisy data once the leading low-rank signal has been removed. Specifically, a rank-r signal matrix fit subtracts the signal energy, leaving a residual diagonal that concentrates around the true noise diagonal as the sample size increases. Pooling these residuals along a fixed feature ordering with a one-dimensional Potts penalty then further denoises within blocks and detects change points: the segmentation introduces a small bias but yields substantial variance reduction, and when jumps are well separated, it accurately recovers both block means and boundaries. Informally, under sub-Gaussian noise, fixed signal

rank, and a bounded aspect ratio, the averaged estimation error of the raw variances estimators is bounded by $O\left(\frac{\log p}{N}\right)$, and the Potts step inherits this consistency when the penalty level is chosen proportional to that rate.

THEOREM 3.1 (Consistency of noise variance estimators). *Suppose Assumption 2.1 and Assumption 2.2 hold. Let $\widehat{C}_n$ be the rank–n fit to $Q = \frac{1}{N}YY^\top$ as in Algorithm 1, define the spectral truncation residual diagonal $\widehat{\sigma} := \mathrm{diag}(Q - \widehat{C}_n)$, and let $\widehat{\sigma}^{\mathrm{pwc}}$ be defined as in (6) with $\beta = c\,\frac{\log p}{N}$. Then with probability $1 - o(1)$, we have $\frac{1}{p}\left\|\widehat{\sigma}^{\mathrm{pwc}} - \sigma\right\|_2^2 \lesssim \frac{\log p}{N}$.*

The rate of convergence $\frac{\log p}{N}$ essentially follows from the concentration of the spectral truncation residual diagonal $\widehat{\sigma}^{\mathrm{raw}}$ and a Potts oracle inequality with $\beta = c\log p/N$ [8]; proofs and precise constants are deferred to the Supplement. In practice, we found the procedure to be robust with respect to the choice of c across a broad range; unless otherwise stated, we use the default value $c = 10$ in our own implementation.

Empirically, we find that the Potts segmentation step in our algorithm significantly improves the initial variance estimates $\widehat{\sigma}$. Detailed numerical results from the simulation studies are provided in the Supplement (Section C.5). Notably, Figure B of the Supplement shows, with a properly chosen penalty parameter β, the Potts-smoothed estimators achieve a mean squared error nearly an order of magnitude smaller than that of the raw residual estimators.

3.2. *Manifold similarity inference using nMSD.* Building on the above noise variance estimators and the spectral properties of the signal matrix outlined in Section 2.4, we develop an estimator of the nMSD between two noisy datasets, enabling statistical inference of manifold similarity between them.

Before proceeding further, we clarify the notation used in the next few sections. We define the total population covariance matrix as $\tilde{\Sigma} = \frac{1}{N}\mathbb{E}[YY^\top]$, where the expectation is with respect to both the noise distribution and the signal distribution ρ from the latent manifold model, and denote $(\xi_k, \tilde{\psi}_k)$ as its eigenpairs. Similarly, conditional on the noiseless samples S_{samp}, we define $\widetilde{\Sigma}^{\mathrm{S}} = \frac{1}{N}\mathbb{E}[YY^\top | S_{\mathrm{samp}}]$ as the conditional population covariance matrix, and denote $(\xi_k^{\mathrm{S}}, \psi_k)$ as its eigenpairs. Note that $\tilde{\Sigma}$ and $\widetilde{\Sigma}^{\mathrm{S}}$ are different from the population and empirical signal covariance matrices M and $\widehat{M}$ defined in (5) as the latter ones are defined for the noiseless samples $S_1, ..., S_N$ only.

For a spike location $\xi^{\mathrm{S}} \notin \{\sigma_1, \ldots, \sigma_p\}$, define functions

$$(7) \qquad A(\xi^{\mathrm{S}}) := (\Sigma - \xi^{\mathrm{S}} I_p)^{-1} = \mathrm{diag}\left(\frac{1}{\sigma_1 - \xi^{\mathrm{S}}}, \ldots, \frac{1}{\sigma_p - \xi^{\mathrm{S}}}\right),$$

and

$$(8) \qquad g(\xi^{\mathrm{S}}) := \frac{1}{p}\,\mathrm{Tr}\,A(\xi^{\mathrm{S}}), \qquad s_2(\xi^{\mathrm{S}}) := \mathrm{Tr}\,A(\xi^{\mathrm{S}})^2.$$

Fix any matrix $U \in \mathbb{R}^{p \times r}$ with orthonormal columns, i.e. $U^\top U = I_r$, and define

$$G_U(\psi) := U^\top A(\psi)U \in \mathbb{R}^{r \times r}.$$

Let $\{\lambda_k\}$ be the eigenvalues of the sample covariance matrix $Q = \frac{1}{N}YY^\top$, and let $\{\theta_k\}$ denote the theoretical limits of $\{\lambda_k\}$ conditional on the noiseless samples S_{samp} as $(N, p) \to \infty$; in particular, as will be discussed in Lemma 4.1 and Lemma 4.2, θ_k is uniquely determined by the conditional population covariance eigenvalues $\{\xi_k^{\mathrm{S}}\}$, the noise covariance Σ and the aspect ratio limit φ. Assuming Σ and φ are known, with a slight abuse of notation we can write $\theta_k := \theta(\xi^{\mathrm{S}})$ so that $\lambda_k \approx \theta(\xi^{\mathrm{S}})$. When $\theta(\cdot)$ is known or estimable from the data, we

can thus construct an estimator of the conditional population covariance eigenvalue ξ^{S} via the inverse map $\widehat{\xi^{S}}_k := \theta^{-1}(\lambda_k)$ for $k = 1, \ldots, r$, and subsequently obtain its standard error estimates by deriving a central limit theorem (CLT) of this estimator.

From this section onward, we also impose a basic signal-strength condition on the spikes of the conditional population covariance matrix Σ^{S}:

ASSUMPTION 3.1 (Signal strength). The leading r eigenvalues $\{\xi^{S}_k\}_{k \leq r}$ of Σ^{S} are supercritical and mutually separated; in particular, each ξ^{S}_k lies outside the bulk spectrum of the noise covariance and is separated from the remaining eigenvalues by a fixed gap.

A precise formulation of the supercriticality and separation conditions, including explicit inequalities on the spike eigenvalues relative to the noise bulk edge, is given in Section D of the Supplementary Material. Assumption 3.1 ensures that the leading r spikes of the conditional population covariance Σ^{S} generate detectable outlier eigenvalues in the sample covariance matrix. In particular, each ξ^{S}_k remains bounded away from the noise bulk and from other spikes as $(N, p) \to \infty$, so that both the outlier map $\theta(\cdot)$ and its inverse $\theta^{-1}(\cdot)$ are well defined and smooth in a neighborhood of these points. This condition is standard in spiked covariance models and is necessary for obtaining consistent estimation and asymptotic normality of the signal–strength estimators.

For given datasets Y_1 and Y_2, to estimate their latent nMSD $d_r(\rho_1, \rho_2)$, inspired by Proposition 2.7, we first construct estimators of the leading empirical signal covariance eigenvalues $\{d_k^2/N\}$, and use them to approximate the population covariance eigenvalues $\{\mathcal{D}_k\}$; these estimates are then substituted into the definition of the nMSD. The procedure proceeds as follows. First, we leverage the estimated noise covariance $\widehat{\Sigma}$ from Algorithm 1 and the top sample covariance eigenvalues λ_j, inverting the outlier eigenvalue map θ, to obtain estimators $\widehat{\xi^{S}}_j$ of the leading conditional population covariance eigenvalues; the concrete expressions of θ and θ' are given by (14). Second, we convert the conditional population covariance eigenvalues into the empirical signal covariance eigenvalues by solving the following secular equations

$$(9) \qquad \det\big(I_r + D_r^2\, G_{U_r}(\xi^{S}_j)\big) = 0, \quad j = 1, 2, \ldots, r,$$

for unknown $D_r = \operatorname{diag}(d_1, d_2, ..., d_r)$, where $U_r \in \mathbb{R}^{p \times r}$ contains the top r left singular vectors of S_{samp}. Once the solution to (9) is obtained, denoted as $\{\widehat{d}_j\}$, we calculate the normalized signal strength vector $\widehat{\Pi}_r = \big(\widehat{d}_1^2, \ldots, \widehat{d}_r^2\big)/\sum_{j=1}^{r} \widehat{d}_j^2 \in \Delta^{r-1}$ and compute the distance estimator. Importantly, the double-processing by the inversion map $\theta^{-1}(\cdot)$ and the secular equations (9) accurately adjust for the intrinsic bias in the sample eigenvalues $\{\lambda_k\}$ caused by the high dimensionality reflected by the non-vanishing φ and the noise heteroskedasticity. Further technical details, regarding the derivation of the secular equations and the exact expression of $\theta(\cdot)$ are provided in Sections 4.1 and 4.2.

To enable efficient computation of the final nMSD estimator, we propose an algorithm that implements the estimation procedure described above (Algorithm 2). Notably, solving the original secular system in (9) requires knowledge of the true signal singular subspace U_r, which is typically unavailable in practice. To overcome this challenge, we adopt a noninformative prior on U_r and show that under this assumption, $G_{U_r}(\xi)$ can be well approximated by $g(\xi)I_r$, which is independent of U_r (Lemma 4.3). This observation substantially simplifies the secular system (Proposition 4.4) and enables a practical and computationally efficient implementation of the algorithm.

Algorithm 2: nMSD estimation procedure

Inputs: data matrix $Y_k \in \mathbb{R}^{p \times N_k}, k = 1, 2$; working rank $r \geq 1$; estimated diagonal noise covariance
$\widehat{\Sigma}_k = \mathrm{diag}(\widehat{\sigma}_{1,k}, \ldots, \widehat{\sigma}_{p,k}), k = 1, 2$.

Output: $\widehat{\Pi}_{r,1}, \widehat{\Pi}_{r,2} \in \Delta^{r-1}$ and the estimated nMSD $\|\widehat{\Pi}_{r,1} - \widehat{\Pi}_{r,2}\|_2$

1. Sample spikes: Form $Q_k = \frac{1}{N_k} Y_k Y_k^\top$ and let $\lambda_{1,k} \geq \cdots \geq \lambda_{r,k}$ be its top r eigenvalues.

2. Invert the outlier map θ: For $j = 1, \ldots, r$ and $k = 1, 2$, solve the scalar equation
$\theta\left(s; \widehat{\Sigma}_k, \varphi_k = p/N_k\right) = \lambda_{j,k}$ for $s > \max_i \widehat{\sigma}_{i,k}$, and set $\widehat{\xi^{\mathrm{S}}}_{j,k} \leftarrow s$.

3. Calculate signal strengths: For each $j = 1, \ldots, r$, set $\widehat{d}_{j,k}^2 = -\frac{1}{\widehat{g}(\widehat{\xi^{\mathrm{S}}}_{j,k})}$ where

$\widehat{g}(s) = \frac{1}{p} \sum_{i=1}^p \frac{1}{\widehat{\sigma}_{i,k} - s}$, for all $s > \max_i \widehat{\sigma}_{i,k}$.

4. Calculate principal variance profiles: For $k = 1, 2$, set $\widehat{\Pi}_{r,k} = \dfrac{(\widehat{d}_{1,k}^2, \ldots, \widehat{d}_{r,k}^2)}{\sum_{i=1}^r \widehat{d}_{i,k}^2}$.

5. Calculate distance estimator: return $\|\widehat{\Pi}_{r,1} - \widehat{\Pi}_{r,2}\|_2$

Our next theorem establishes the consistency of the empirical signal covariance eigenvalue, normalized principal variance profile, and nMSD estimation based on Algorithm 2.

THEOREM 3.2 (Consistency of nMSD estimator). *Under Assumption 2.1, Assumption 2.2 and Assumption 3.1, fix $r \geq 1$. Let $\{\widehat{\xi^{\mathrm{S}}}_j\}_{j=1}^r$ be any consistent estimators of the conditional population spikes $\{\xi_j^{\mathrm{S}}\}_{j=1}^r$ (e.g., by inverting the outlier map), and let $\widehat{\Sigma}$ be a consistent estimator of the diagonal noise Σ. Consider the empirical secular system obtained by replacing $(\xi_j^{\mathrm{S}}, \Sigma)$ with $(\widehat{\xi^{\mathrm{S}}}_j, \widehat{\Sigma})$ in (9). If this system admits a solution $\widehat{D}_r^2 = \mathrm{diag}(\widehat{d}_1^2, \ldots, \widehat{d}_r^2)$, then*

$$(10) \qquad \widehat{d}_j^2 \xrightarrow{\mathbb{P}} d_j^2 \quad (j = 1, \ldots, r), \qquad \widehat{\Pi}_r := \frac{\widehat{d}^2}{\mathbf{1}^\top \widehat{d}^2} \xrightarrow{\mathbb{P}} \Pi_r := \frac{d^2}{\mathbf{1}^\top d^2}.$$

Consequently, for two independent datasets generated under the same framework,

$$\left\|\widehat{\Pi}_{r,1} - \widehat{\Pi}_{r,2}\right\|_2 \xrightarrow{\mathbb{P}} d_r(\rho_1, \rho_2).$$

Furthermore, assume that U_r is obtained as the first r columns of a random orthogonal matrix Q drawn from the Haar distribution on $\mathbb{O}(p)$. Then the secular system admits the following closed-form solution:

$$(11) \qquad \widehat{d}_j^2 = -\frac{1}{\widehat{g}(\widehat{\xi^{\mathrm{S}}}_j)}, \qquad \widehat{g}(s) = \frac{1}{p} \sum_{i=1}^p \frac{1}{\widehat{\sigma}_i - s}, \quad j = 1, \ldots, r,$$

which also satisfies $\widehat{d}_j^2 \xrightarrow{\mathbb{P}} d_j^2$ and hence $\widehat{\Pi}_r \xrightarrow{\mathbb{P}} \Pi_r$ as above.

Note that our framework is not restricted to the case where U_r follows a Haar distribution. In cases where U_r has a different prior distribution encoding additional structural knowledge, we may apply a similar argument to approximate $G_{U_r}(\xi)$ by some deterministic matrix independent of U_r. When such a reduction is infeasible, one can always apply Bayesian Monte Carlo methods to obtain numerical solutions for $\{d_j\}$. Equation (10) of Theorem 3.2 ensures that, in all such cases, the proposed estimators remain consistent.

In addition to the estimation consistency, the proposed nMSD estimator, as well as the components of $\widehat{\Pi}_r$, also admit asymptotic normality properties , which are derived in detail in

Section 4.4. Building on the asymptotic normality, we can construct confidence intervals for the components of Π_r and the underlying nMSD between two datasets, providing uncertainty quantification of our estimators.

Let $\widehat{\Pi}_{r,k} \in \Delta^{r-1}$ be the principal variance profile estimators from Algorithm 2. Let $\widehat{V}_\Pi$ denote any estimator of the asymptotic covariance $\mathrm{Cov}(\widehat{\Pi}_r)$ that is consistent in the sense that $[\widehat{V}_\Pi]_{tt} \xrightarrow{\mathbb{P}} [\Sigma_\Pi]_{tt}/N$ for each fixed t. A convenient plug–in implementation, obtained by replacing population quantities in the variance formulas with their empirical counterparts, is given in Section 4.3, see in particular Equation (33).

For $\alpha \in (0,1)$ and $z_{1-\alpha/2}$ the standard normal $\alpha/2$-percentile, we define the component-wise $(1-\alpha)$ confidence intervals

$$\mathrm{CI}_t^{(\Pi)} := \left[(\widehat{\Pi}_r)_t \pm z_{1-\alpha/2} \sqrt{[\widehat{V}_\Pi]_{tt}} \right], \qquad t = 1, \ldots, r,$$

which satisfy $\mathrm{Pr}\big((\Pi_r)_t \in \mathrm{CI}_t^{(\Pi)}\big) \to 1 - \alpha$ as $(N, p) \to \infty$, for any given t.

Similarly, for two independent datasets producing $\widehat{\Pi}_{r,1}$ and $\widehat{\Pi}_{r,2}$ with covariance estimates $\widehat{V}_\Pi^{(1)}$ and $\widehat{V}_\Pi^{(2)}$–see Section 4 and particularly Equation(33) for their detailed expressions–the difference $\Delta\widehat{\Pi} := \widehat{\Pi}_{r,1} - \widehat{\Pi}_{r,2}$ admits plug-in covariance estimates $\widehat{V}_\Delta := \widehat{V}_\Pi^{(1)} + \widehat{V}_\Pi^{(2)}$. Hence the componentwise $(1-\alpha)$ CIs for $\Delta\Pi$ can be constructed as

$$\mathrm{CI}_t^{(\Delta)} := \left[(\Delta\widehat{\Pi})_t \pm z_{1-\alpha/2} \sqrt{[\widehat{V}_\Delta]_{tt}} \right].$$

Lastly, let $d_r(\rho_1, \rho_2) := \|\Pi^{(1)} - \Pi^{(2)}\|_2$ and $\widehat{d_r(\rho_1, \rho_2)} := \|\Delta\widehat{\Pi}\|_2$. When $\widehat{d}_r$ is bounded away from 0, we can construct a $(1-\alpha)$-level CI for nMSD $d_r(\rho_1, \rho_2)$ as

$$\mathrm{CI}_{\mathrm{nMSD}} = \left[\widehat{d_r(\rho_1, \rho_2)} \pm z_{1-\alpha/2} \sqrt{\frac{\Delta\widehat{\Pi}^\top \widehat{V}_\Delta \Delta\widehat{\Pi}}{\widehat{d_r(\rho_1, \rho_2)}^2}} \right].$$

PROPOSITION 3.3. *Under Assumption 2.1, Assumption 2.2 and Assumption 3.1, we have* $\mathrm{Pr}\big(d_r(\rho_1, \rho_2) \in \mathrm{CI}_{\mathrm{nMSD}}\big) \to 1 - \alpha$ *as* $(N, p) \to \infty$.

3.3. *Manifold alignability inference.* A closely related problem in comparing datasets is assessing whether they share a common latent manifold structure—what we referred to as the manifold alignability problem. Within our manifold spectrometrics framework, this problem can be naturally formulated as a hypothesis testing task, where the null hypothesis states that the two datasets possess identical normalized principal variance profiles:

$$H_0 : \ \Pi_r(\rho_1) = \Pi_r(\rho_2).$$

From the estimation pipeline above, obtain the normalized vectors $\widehat{\Pi}_{r,i} \in \Delta^{r-1}$ and their plug-in covariances $\widehat{V}_{\Pi,i}$ via (33) (for $i = 1, 2$). Let $\Delta_\Pi := \widehat{\Pi}_{r,1} - \widehat{\Pi}_{r,2}$. Define the test statistic

(12) $$T_\Pi := \Delta_\Pi^\top \big(\widehat{V}_{\Pi,1} + \widehat{V}_{\Pi,2}\big)^+ \Delta_\Pi$$

Here each $\widehat{V}_{\Pi,k} = O_p(N_k^{-1})$, and we use the Moore–Penrose inverse because $V_\Pi \mathbf{1} = \mathbf{0}$ and $\mathrm{rank}(V_\Pi) = r - 1$. By Theorem 3.4 below, under H_0 we have $T_\Pi \xrightarrow{d} \chi_{r-1}^2$; thus for a target significance level α_{sig}, an asymptotically valid test is to reject H_0 if $T_\Pi > \chi_{r-1, 1-\alpha_{\mathrm{sig}}}^2$, which is the upper $1 - \alpha_{\mathrm{sig}}$ percentile of the χ_{r-1}^2-distribution.

When H_0 is rejected, we conclude that the two distributions ρ_1 and ρ_2 underlying Y_1 and Y_2 respectively, have different signal strengths profiles. If H_0 is not rejected, the data are

compatible with a common signal up to the invariances of our metric (e.g., an orthogonal rotation of the ambient coordinates and a common global scale), though failure to reject does not necessarily imply $\rho_1 = \rho_2$. We now present the formal theoretical guarantees for size and power of the proposed alignability test.

THEOREM 3.4 (Null limit). *Under Assumption 2.1, 2.2 and 3.1 with* $H_0 : \Pi_r(\rho_1) = \Pi_r(\rho_2)$, *we have* $T_\Pi \xrightarrow{d} \chi^2_{r-1}$.

THEOREM 3.5 (Power under fixed alternatives). *Under Assumption 2.1, 2.2 and 3.1, if* $\Delta := \Pi_r(\rho_1) - \Pi_r(\rho_2) \neq 0$, *then for* $N_{\text{eff}} = \frac{N_1 N_2}{N_1 + N_2}$, *we have* $\frac{T_\Pi}{N_{\text{eff}}} \xrightarrow{p} c_0 := \Delta^\top V_\Delta^+ \Delta > 0$. *Consequently, for any* $\varepsilon \in (0, c_0)$, *we have* $\Pr\{T_\Pi \geq N_{\text{eff}}(c_0 - \varepsilon)\} \rightarrow 1$. *Moreover, let* $Z \sim \chi^2_{r-1}$ *denote a chi-square random variable with* $r - 1$ *degrees of freedom. Then, for all* $x > 0$, *we have* $\Pr\{Z \geq x\} \leq \exp\left(-\frac{1}{2}\left[x - (r-1) - (r-1)\ln\{x/(r-1)\}\right]\right)$, *that is, the p-value decays as* $\exp\{-\frac{N_{\text{eff}}}{2}(c_0 - \varepsilon) + o(N_{\text{eff}})\}$.

COROLLARY 3.6 (Separation–driven power bound). *Under the setting of Theorem 3.5, let* $\lambda_{\max}(V_\Delta)$ *be the largest nonzero eigenvalue of* V_Δ. *Then it holds that* $c_0 = \Delta^\top V_\Delta^+ \Delta \geq \frac{\|\Delta\|_2^2}{\lambda_{\max}(V_\Delta)}$. *Hence, if* $\|\Pi_r(\rho_1) - \Pi_r(\rho_2)\|_2 \geq C > 0$, *then with high probability* $T_\Pi \gtrsim N_{\text{eff}} \frac{C^2}{\lambda_{\max}(V_\Delta)}$, *and the p-value decays as* $\exp\{-\frac{N_{\text{eff}}}{2} C^2/\lambda_{\max}(V_\Delta)\}$ *up to polylog factors.*

Theorem 3.4 establishes the asymptotic null distribution of the test statistic, providing a principled test for the equality of underlying structures across datasets. The procedure accommodates heterogeneous noise covariances and unequal sample sizes, while the effective sample size N_{eff} and weight $\alpha = N_2/(N_1 + N_2)$ determine how each dataset contributes. Theorem 3.5 establishes power consistency and shows that, under fixed alternatives, the p-value decays exponentially in the effective sample size: p-value $= \exp\{-\frac{N_{\text{eff}}}{2} c_0 + o(N_{\text{eff}})\}$, with $c_0 = \Delta^\top V_\Delta^+ \Delta$. By Corollary 3.6, we have $c_0 \geq \|\Delta\|_2^2/\lambda_{\max}(V_\Delta)$, which means larger separation $\|\Delta\|_2$ between the two manifolds yields a faster exponential decay and hence higher power. In Section 5, we compare our test with alternative methods and demonstrate that it consistently achieves superior performance whenever a nonzero spectral distance exists between the underlying manifolds.

3.4. *Extension to kernel-based manifold learning.* In many applications, similarities between datasets may only become apparent after a nonlinear feature transformation. Our manifold spectral framework naturally extends to such settings through the use of reproducing kernel Hilbert spaces (RKHS). In this part, we formulate the RKHS version of our distance measure, working entirely with Gram matrices to maintain consistency with the covariance-based perspective adopted throughout the paper. We define the key quantities and state the main results, while deferring detailed proofs to Section M of the Supplement. The arguments follow standard kernel spectral theory [17, 39] and are analogous to those in the linear setting.

RKHS setup. Let $(\mathcal{X}, \mathcal{B})$ be a measurable space and $K : \mathcal{X} \times \mathcal{X} \to \mathbb{R}$ a Mercer kernel with reproducing kernel Hilbert space (RKHS) $\mathcal{H}_K$ and feature map $\phi : \mathcal{X} \to \mathcal{H}_K$ satisfying $K(x,y) = \langle \phi(x), \phi(y) \rangle_{\mathcal{H}_K}$, and $\kappa^2 := \sup_{x \in \mathcal{X}} K(x,x) < \infty$. For dataset $k \in \{1,2\}$, let ρ_k be the distribution of X_k on $\mathcal{X}$ and define the (centered) population kernel covariance operator $M_{K,k} := \mathbb{E}_{X \sim \rho_k}\left[(\phi(X) - m_k) \otimes (\phi(X) - m_k)\right]$, with $m_k := \mathbb{E}_{X \sim \rho_k}[\phi(X)]$, where $(u \otimes v)f := \langle f, v \rangle_{\mathcal{H}_K} u$. By boundedness of K, each $M_{K,k}$ is self-adjoint, positive, and trace-class. Let $(\mathcal{D}_{k,j})_{j \geq 1}$ be the eigenvalues of $M_{K,k}$ arranged in nonincreasing order. We assume a spiked structure for the leading r components: for some fixed $r \geq 1$ and each k, the top r eigenvalues are strictly positive and separated, that is, $\mathcal{D}_{k,1} \geq \cdots \geq \mathcal{D}_{k,r} > \mathcal{D}_{k,r+1}$, and $\min_{1 \leq j \leq r}(\mathcal{D}_{k,j} - \mathcal{D}_{k,j+1}) \geq \gamma_k > 0$.

Kernelized manifold spectral distance. In analogy with Definition 2.2 and Definition 2.3, we define the top-r kernel principal-variance vector $\mathcal{D}_k^{(r)} := (\mathcal{D}_{k,1}, \ldots, \mathcal{D}_{k,r})^\top$, $\Pi_r^{(K)}(\rho_k) := \frac{\mathcal{D}_k^{(r)}}{\mathbf{1}^\top \mathcal{D}_k^{(r)}} \in \Delta^{r-1}$, and the *kernelized manifold spectral distance*

$$(13) \qquad d_r^{(K)}(\rho_1, \rho_2) := \left\| \Pi_r^{(K)}(\rho_1) - \Pi_r^{(K)}(\rho_2) \right\|_2.$$

This distance compares the relative allocation of variance across the leading r eigendirections of $M_{K,k}$ in the feature space $\mathcal{H}_K$. It is invariant under unitary transformations of $\mathcal{H}_K$ and under a common global rescaling of the kernel K. For the linear kernel $K(x, y) = \langle x, y \rangle$, $d_r^{(K)}$ reduces to the manifold spectral distance in Definition 2.3.

Sample-based construction via Gram matrices. Given observations $\{x_{k,1}, \ldots, x_{k,N_k}\}$ from ρ_k, let K_k be the $N_k \times N_k$ kernel matrix with entries $[K_k]_{ij} = K(x_{k,i}, x_{k,j})$ and let $\widetilde{K}_k$ be its standard centered version in feature space. Define the normalized Gram matrix $G_k := \frac{1}{N_k} \widetilde{K}_k$. It is straightforward that the nonzero eigenvalues of G_k coincide with those of the empirical kernel covariance operator $\widehat{M}_{K,k} := \frac{1}{N_k} \sum_{i=1}^{N_k} \big(\phi(x_{k,i}) - m_k\big) \otimes \big(\phi(x_{k,i}) - m_k\big)$, so that all spectral quantities of interest can be computed from G_k. Let $\hat{\mathcal{D}}_{k,1} \geq \cdots \geq \hat{\mathcal{D}}_{k,r} > 0$ be the leading r eigenvalues of G_k, and define the empirical kernel spectral profile $\widehat{\Pi}_{r,k}^{(K)} := \frac{(\hat{\mathcal{D}}_{k,1}, \ldots, \hat{\mathcal{D}}_{k,r})}{\sum_{j=1}^{r} \hat{\mathcal{D}}_{k,j}} \in \Delta^{r-1}$, together with the plug-in estimator of (13), which is given by $\hat{d}_r^{(K)} := \left\| \widehat{\Pi}_{r,1}^{(K)} - \widehat{\Pi}_{r,2}^{(K)} \right\|_2$.

Consistency of the kernelized manifold spectral estimator. We work in the regime where $N_k \to \infty$ with fixed r. Under the bounded-kernel assumption, the spectral perturbation bound $\|\widehat{M}_{K,k} - M_{K,k}\|_{\mathrm{op}} = O_\mathbb{P}(N_k^{-1/2})$ holds, and the spiked eigenvalues of $M_{K,k}$ are stable. Consequently, for each fixed $j \leq r$, we have $\hat{\mathcal{D}}_{k,j} \xrightarrow{\mathbb{P}} \mathcal{D}_{k,j}$, $\widehat{\Pi}_{r,k}^{(K)} \xrightarrow{\mathbb{P}} \Pi_r^{(K)}(\rho_k)$, and therefore $\hat{d}_r^{(K)} \xrightarrow{\mathbb{P}} d_r^{(K)}(\rho_1, \rho_2)$.

4. Technical details behind our main results. In this section, we present the technical foundations of our main results, focusing on the theoretical derivation of the manifold estimator and the corresponding variance estimation. Detailed proofs of the main theorems are provided in the Supplement. The analysis is conducted under Assumptions 2.1, 2.2 and 3.1.

In Section 4.1, we first establish delocalization properties of the signal representation and derive the outlier eigenvalue CLT conditional on the signal matrix. In Section 4.2, under the Haar distribution assumption, we decouple the rank-r secular equations and recover the signal strengths in closed form. Sections 4.3 and 4.4 derive the variance decomposition of the outlier eigenvalues into noise- and signal-related components, connected through the outlier map θ, and uses this result to obtain the asymptotic distribution of $\hat{d}^2$ and the normalized vector $\widehat{\Pi}$. Finally, Section 4.5 constructs consistent plug-in estimators for the residual moments and covariance components required to implement the proposed inference procedures.

4.1. *Conditional eigenvalue CLT for sample covariances.*

LEMMA 4.1 (Delocalization). *Let* $\widetilde{\Sigma}^\mathrm{S} = \Sigma + \frac{S_{\mathrm{samp}} S_{\mathrm{samp}}^\top}{N}$ *and let* ψ_k *be a unit eigenvector of* $\widetilde{\Sigma}^\mathrm{S}$ *associated with an outlier* ξ_k^S. *Set* $B = \frac{S_{\mathrm{samp}}^\top \psi_k}{\sqrt{N}} \in \mathbb{R}^N$. *Under Assumption 2.1, 2.2 and 3.1, with probability* $1 - o(1)$, *we have* $\|B\|_\infty \leq C_V \frac{\|D_{\mathrm{samp}}\|_{\mathrm{op}} \sqrt{n \log N}}{\sqrt{N}}$ *where* C_V *is a constant.*

This lemma could be proved with the delocalization of V_{samp} in Proposition 2.7 and the low rank property of S_{samp} in Proposition 2.6. Based on this lemma we could derive the asymptotic normality of λ_k using the recent random matrix theory results [29].

Under Assumption 2.1,2.2 and 3.1, the deterministic outlier map and its derivative are

$$(14) \qquad \theta(\xi) \;=\; \xi \;+\; \frac{1}{N}\,\mathrm{tr}\!\left(\frac{\xi\,\Sigma}{\xi - \Sigma}\right), \qquad \theta'(\xi) \;=\; 1 \;-\; \frac{1}{N}\,\mathrm{tr}\!\left(\frac{\Sigma^2}{(\xi - \Sigma)^2}\right).$$

Fix r and let $\xi_1^{\mathrm{S}} > \cdots > \xi_r^{\mathrm{S}}$ be separated outliers of $\widetilde{\Sigma}^{\mathrm{S}} = \Sigma + \frac{S_{\mathrm{samp}}S_{\mathrm{samp}}^{\top}}{N}$ with associated unit eigenvectors $\psi_1, \ldots, \psi_r$. For $k \le r \le d$ write

$$a_k := \psi_k^{\top} \Sigma \psi_k, \qquad b_k := \psi_k^{\top} S_{\mathrm{samp}} S_{\mathrm{samp}}^{\top} \psi_k / N = \xi_k^{\mathrm{S}} - a_k, \qquad \theta_k' := \theta'(\xi_k^{\mathrm{S}}),$$

and denote by $\kappa_3 := \mathbb{E}[(X_{i\mu})^3]$ and $\kappa_4 := \mathbb{E}[(X_{i\mu})^4] - 3$ the third and fourth cumulants of the standardized noise entries. For vectors $u, v \in \mathbb{R}^p$ set $M_{2,2}(u,v) := \sum_{i=1}^p u_i^2 v_i^2$.

LEMMA 4.2 (Conditional CLT for sample covariance outlier eigenvalues [29]).   *Under Assumption 2.1, Assumption 2.2 and Assumption 3.1 and conditional on S_{samp}, we have*

$$(15) \qquad\qquad \sqrt{N}\left(\lambda_k - \theta(\xi_k^{\mathrm{S}})\right) \;=\; \Phi_k \;+\; \Theta_k \;+\; L_k \;+\; o_{\mathbb{P}}(1),$$

where $\mathbb{E}[\Phi_k \mid S_{\mathrm{samp}}] = \mathbb{E}[\Theta_k \mid S_{\mathrm{samp}}] = 0$, and $L_k \equiv 0$ if $\kappa_3 = 0$. Moreover, for each fixed k, conditional on S_{samp} the term Φ_k is asymptotically normal as $N \to \infty$.

The conditional second moments admit the block decomposition

$$(16) \qquad \mathrm{Var}(\Phi_k \mid S_{\mathrm{samp}}) = V_{kk}^{(G)} \;+\; \kappa_4\,(\theta_k')^2\, M_{2,2}\!\left(\Sigma^{1/2}\psi_k, \Sigma^{1/2}\psi_k\right) \;+\; o(1),$$

$$(17) \qquad \mathrm{Cov}(\Phi_k, \Theta_k \mid S_{\mathrm{samp}}) = W_{kk} \;+\; o(1), \qquad W_{kk} = \kappa_3\,(\theta_k')^2\, a_k\, b_k,$$

$$(18) \qquad \mathrm{Var}(\Theta_k \mid S_{\mathrm{samp}}) = 4\,(\theta_k')^2\, a_k\, b_k,$$

with the Gaussian block

$$(19) \qquad\qquad V_{kk}^{(G)} \;=\; 2\,(\theta_k')^2 a_k^2 \;+\; 2\,\xi_k^{\mathrm{S}2} \theta_k' \;-\; 2\,\xi_k^{\mathrm{S}2}(\theta_k')^2.$$

Consequently,
(20)
$$\mathrm{Var}(\lambda_k \mid S_{\mathrm{samp}}) = \frac{1}{N}\left(V_{kk}^{(G)} + \kappa_4\,(\theta_k')^2\, M_{2,2}\!\left(\Sigma^{1/2}\psi_k, \Sigma^{1/2}\psi_k\right) + 2\,W_{kk} + 4\,(\theta_k')^2\, a_k\, b_k\right) + o\!\left(\frac{1}{N}\right).$$

In particular, if the noise is symmetric ($\kappa_3 = 0$) then $W_{kk} = 0$; if it is Gaussian ($\kappa_3 = \kappa_4 = 0$) then only $V_{kk}^{(G)}$ and $4(\theta_k')^2 a_k b_k$ remain.

This lemma shows that the gap between the sample eigenvalue λ and its corresponding limit θ could be further divided into three parts. To eventually derive the asymptotic normality of the nMSD estimator, we need the right-hand side of (15) to be asymptotically normal. The first term Φ has been proved to be asymptotically normal and the third part is zero under Assumption 2.1. The second term, however, is not asymptotically normal in general. Under our latent manifold model, we establish a delocalization property of $\frac{S_{\mathrm{samp}}^{\top}\psi_k}{\sqrt{N}}$ using Lemma 4.1 and Proposition 2.7, which ensures the asymptotic normality of Θ_k.

4.2. *Solving secular equations.* Let $D_r = \mathrm{diag}(d_1, \ldots, d_r)$ collect the unknown signal strengths so that $S_{\mathrm{samp}} S_{\mathrm{samp}}^\top / N = U_r D_r^2 U_r^\top$. And Let $U_r \in \mathbb{R}^{p \times r}$ be Haar distributed on $\{U \in \mathbb{R}^{p \times r} : U^\top U = I_r\}$, independently of Σ. Set

$$G_{U_r}(\xi) := U_r^\top A(\xi) U_r \in \mathbb{R}^{r \times r}, \qquad R(\xi) := G_{U_r}(\xi) - g(\xi) I_r.$$

Using the outlier map (14), we can invert the sample spikes λ_k to obtain estimates of the conditional population spikes ξ_k^{S}. Our ultimate target, however, is the signal strengths d_k^2. These are linked to ξ_k^{S} through $\Sigma + \frac{S_{\mathrm{samp}} S_{\mathrm{samp}}^\top}{N} = \widetilde{\Sigma}^{\mathrm{S}}$, because d_k^2 are the eigenvalues of $\frac{S_{\mathrm{samp}} S_{\mathrm{samp}}^\top}{N}$, whereas ξ_k^{S} are the eigenvalues of $\widetilde{\Sigma}^{\mathrm{S}}$. For any $\xi_j^{\mathrm{S}} \notin \mathrm{spec}(\Sigma)$, the matrix determinant lemma (Sylvester's identity) gives:

$$\det\big(\Sigma + U_r D_r^2 U_r^\top - \xi_j^{\mathrm{S}} I_p\big) = \det(\Sigma - \xi_j^{\mathrm{S}} I_p) \det\big(I_r + D_r^2 U_r^\top (\Sigma - \xi_j^{\mathrm{S}} I_p)^{-1} U_r\big)$$

$$= \det(\Sigma - \xi_j^{\mathrm{S}} I_p) \det\big(I_r + D_r^2 G_{U_r}(\xi_j^{\mathrm{S}})\big).$$

Hence ξ_j^{S} is an eigenvalue of $\Sigma + U_r D_r^2 U_r^\top$ if and only if

$$\det\big(I_r + D_r^2 G_{U_r}(\xi_j^{\mathrm{S}})\big) = 0, \quad j = 1, 2, \ldots, r.$$

Our next lemma shows that the matrix $G_{U_r}(\xi_j^{\mathrm{S}})$ can be well approximated by a diagonal matrix $g(\xi_j^{\mathrm{S}}) I_r$ independent of U_r, thereby providing a means to simplify the secular system and derive its closed-form solution.

LEMMA 4.3 (Concentration of $G_{U_r}(\xi)$). *Under Assumptions 2.1, 2.2 and 3.1, with $U_r \sim$ Haar on $\{U \in \mathbb{R}^{p \times r} : U^\top U = I_r\}$ and independent of Σ, we have $\mathbb{E}\big[G_{U_r}(\xi)\big] = g(\xi) I_r$. Moreover, as $(N, p) \to \infty$ with fixed r and $\min_{1 \leq i \leq p} |\sigma_i - \xi| \geq c > 0$, we have*

$$(21) \qquad \big\| R(\xi) \big\|_{\mathrm{op}} = O_{\mathbb{P}}\Big(\frac{\sqrt{s_2(\xi)}}{p} \sqrt{r} + \|A(\xi)\|_{\mathrm{op}} \sqrt{\frac{r}{p}} \Big) = o_{\mathbb{P}}(1),$$

where $\| \cdot \|_{\mathrm{op}}$ denotes the operator norm.

PROPOSITION 4.4 (Exact solution under Haar prior). *Assume the setting of Lemma 4.3 with fixed r. Set $g_j := g(\xi_j^{\mathrm{S}})$ and assume $|g_j| \geq g_{\min} \geq c_0 > 0$. Let $D_r = \mathrm{diag}(d_1, \ldots, d_r)$ solve the secular system (9). If, in addition, the numbers $\{-1/g_j\}_{j=1}^r$ are pairwise separated by at least $\Delta > 0$, then there exists a unique permutation π of $\{1, \ldots, r\}$ such that*

$$(22) \qquad d_{\pi(j)}^2 = -\frac{1}{g_j} + o_{\mathbb{P}}(1), \qquad j = 1, \ldots, r.$$

For each $j = 1, \ldots, r$, write $G_j := G_{U_r}(\xi_j^{\mathrm{S}})$ and $R_j := R(\xi_j^{\mathrm{S}})$. When G_j is replaced by its conditional expectation $g_j I_r$, Equations (9) reduce to $\prod_{\ell=1}^r (1 + g_j d_\ell^2) = 0$ for each j. The unique multiset solution is therefore $\{d_\ell^2\}_{\ell=1}^r = \{-1/g_j\}_{j=1}^r$. Lemma 4.3 extends this mean-field result to a high-probability statement, establishing that $\max_j \|R_j\|_{\mathrm{op}} = o_{\mathbb{P}}(1)$, which in turn yields $d_{\pi(j)}^2 = -1/g_j + o_{\mathbb{P}}(1)$ for some permutation π, as formalized in Proposition 4.4.

4.3. *Unconditional eigenvalue CLT for sample covariances.* A key feature of our data-generating model is that the randomness of the final estimators arises from both the noise and the signal-generating processes. In this section, we first derive the population-level contribution to the asymptotic covariance of the sample eigenvalues λ_k attributable to signal randomness, and then establish the unconditional eigenvalue CLT for the sample covariance.

4.3.1. *Delineating uncertainty due to noiseless samples.* In this subsection we isolate the variability that comes from repeatedly generating noiseless signal samples $S_1, \ldots, S_N$, while keeping the noise covariance Σ fixed. We treat the empirical signal covariance $\widehat{M} = N^{-1} \sum_{i=1}^{N} S_i S_i^\top$ as a random perturbation of its population counterpart M, and use first–order eigenvalue perturbation theory to describe how a simple spike of $\widetilde{\Sigma} = \Sigma + M$ changes when M is replaced by $\widehat{M}$. This shows that, to leading order, the shift of each outlier eigenvalue is governed by a quadratic form of the perturbation taken along its population eigenvector. We then derive explicit formulas for the covariance matrix of these quadratic forms, which will later serve as the "noiseless–sample" component in the overall asymptotic covariance of the sample spikes.

Throughout, remember that $S_i \in \mathbb{R}^p$ denote a random column with $\mathbb{E}\|S_i\|^4 < \infty$, population second moment is represented by $M = \mathbb{E}[S_i S_i^\top]$, and the sample second moment can be calculated by $\widehat{M} = \frac{1}{N} \sum_{i=1}^{N} S_i S_i^\top$. We define the centered fluctuation $\Delta_M := \widehat{M} - M$.

Let $\widetilde{\Sigma} = \Sigma + M$ have a simple outlier eigenvalue ξ_k with a unit eigenvector $\tilde{\psi}_k$, and denote the eigengap by $\gamma_k := \min\{\xi_{k-1} - \xi_k, \ \xi_k - \xi_{k+1}\} > 0$.

LEMMA 4.5 (First-order sensitivity of a simple spike).   *For any symmetric perturbation $E \in \mathbb{R}^{p \times p}$, we have $\lambda_k(\widetilde{\Sigma} + E) - \lambda_k(\widetilde{\Sigma}) = \tilde{\psi}_k^\top E \tilde{\psi}_k + R_k(E)$, and $|R_k(E)| \leq C \frac{\|E\|_{\mathrm{op}}^2}{\gamma_k}$, for a universal constant $C > 0$. In particular, if $\|E\|_{\mathrm{op}} = o(1)$, then the spike shift satisfies $\lambda_k(\widetilde{\Sigma} + E) - \lambda_k(\widetilde{\Sigma}) = \tilde{\psi}_k^\top E \tilde{\psi}_k + o(\|E\|_{\mathrm{op}})$.*

This is the classical Hadamard first–variation formula for simple eigenvalues, together with a second–order remainder bounded by the eigengap. It follows from analytic perturbation theory or by a resolvent expansion plus the Davis–Kahan control of eigenprojections; the gap γ_k ensures differentiability of λ_k at $\widetilde{\Sigma}$. Applying Lemma 4.5 with $E = \Delta_M$ shows that, conditional on (Σ, M) so that $\tilde{\psi}_k$ is deterministic and since $\|\Delta_M\|_{\mathrm{op}} = O_p(N^{-1/2})$,

$$(23) \qquad \delta\xi_k := \lambda_k(\Sigma + \widehat{M}) - \lambda_k(\Sigma + M) = \tilde{\psi}_k^\top \Delta_M \tilde{\psi}_k + o_p(N^{-1/2}).$$

Thus, to first order the spike responds only to the quadratic form of the perturbation Δ_M along its own eigenvector $\tilde{\psi}_k$. The next lemma computes the covariance of those quadratic forms. It is stated for general fixed evaluation directions and then specialized to $v_k = \tilde{\psi}_k$.

LEMMA 4.6 (Quadratic-form covariance).   *Let $v_1, \ldots, v_m \in \mathbb{R}^p$ be fixed unit vectors, independent of the sample $\{S_i\}_{i=1}^{N}$. Define $\delta_k := v_k^\top \Delta_M v_k = \frac{1}{N} \sum_{i=1}^{N} \{(v_k^\top S_i)^2 - \mathbb{E}[(v_k^\top S_i)^2]\}$. Then $\mathbb{E}[\delta_k] = 0$ and the covariance matrix $\Gamma^{(\mathrm{sig})} = (\Gamma_{kj}^{(\mathrm{sig})})$ of $(\delta_1, \ldots, \delta_m)$ satisfies*

$$(24) \qquad \Gamma_{kj}^{(\mathrm{sig})} = \mathrm{Cov}(\delta_k, \delta_j) = \frac{1}{N}\Big\{ \mathbb{E}[(v_k^\top S)^2 (v_j^\top S)^2] - \mathbb{E}[(v_k^\top S)^2] \, \mathbb{E}[(v_j^\top S)^2] \Big\}.$$

Writing the fourth raw–moment tensor $T^{(4)} := \mathbb{E}[S^{\otimes 4}]$ and $b_k := v_k^\top M v_k$, this equals

$$(25) \qquad \Gamma_{kj}^{(\mathrm{sig})} = \frac{1}{N}\langle v_k \otimes v_k \otimes v_j \otimes v_j, \ T^{(4)} \rangle - \frac{1}{N} b_k \, b_j.$$

If, in addition, $\mathrm{Kc} := \mathrm{Cum}_4(S)$ denotes the fourth central cumulant tensor, then

$$(26) \qquad \Gamma_{kj}^{(\mathrm{sig})} = \frac{1}{N}\Big\{ 2\,(v_k^\top M \, v_j)^2 + \mathrm{Kc}[v_k, v_k, v_j, v_j] \Big\}.$$

Combining (23) with Lemma 4.6 specialized to $v_k = \tilde{\psi}_k$, conditional on (Σ, M), we have

$$\sqrt{N}\,\delta\xi_k = \sqrt{N}\,\tilde{\psi}_k^\top \Delta_M \tilde{\psi}_k + o_p(1), \qquad \mathrm{Cov}\big(\tilde{\psi}_k^\top \Delta_M \tilde{\psi}_k, \ \tilde{\psi}_j^\top \Delta_M \tilde{\psi}_j\big) = \Gamma_{kj}^{(\mathrm{sig})} + o(N^{-1}),$$

with $\Gamma^{(\mathrm{sig})}$ given by (26), upon substituting $v_k = \tilde{\psi}_k$. To first order, the spike ξ_k depends only on the quadratic form of Δ_M along its own eigenvector $\tilde{\psi}_k$. Evaluating along any other direction $v \neq \tilde{\psi}_k$ would correspond to the perturbation of an unrelated linear functional and would not capture the spike's first-order behavior. In practice, since neither the true signal eigenvector nor the conditional population eigenvector is observable, we estimate the variance using plug-in sample eigenvectors.

4.3.2. *Unconditional CLT and total asymptotic variance.* Recall that $(\xi_k^{\mathrm{S}}, \psi_k)$ refer to the conditional population eigenpairs of $\widetilde{\Sigma}^{\mathrm{S}}$, in contrast to the population pairs $(\xi_k, \tilde{\psi}_k)$ used in the previous subsection. Fix r and let $\xi_1^{\mathrm{S}} > \cdots > \xi_r^{\mathrm{S}}$ be separated outliers of $\widetilde{\Sigma}^{\mathrm{S}} = \Sigma + \frac{S_{\mathrm{samp}}S_{\mathrm{samp}}^\top}{N}$ with unit eigenvectors $\psi_1, \ldots, \psi_r$. For $k, j \leq r$ write $A_{kj} := \psi_k^\top \Sigma \psi_j$, $B_{kj} := \psi_k^\top S_{\mathrm{samp}} S_{\mathrm{samp}}^\top \psi_j / N$, $a_k := A_{kk}$, $b_k := B_{kk} = \xi_k^{\mathrm{S}} - a_k$, and $\theta_k' := \theta'(\xi_k^{\mathrm{S}})$. Let the standardized noise entries have third and fourth cumulants $\kappa_3 := \mathbb{E}[(X_{i\mu})^3]$ and $\kappa_4 := \mathbb{E}[(X_{i\mu})^4] - 3$, and set $M_{2,2}(u,v) := \sum_{i=1}^p u_i^2 v_i^2$ for $u, v \in \mathbb{R}^p$. The next proposition concerns the unconditional CLT for the eigenvalues of the sample covariance matrix.

PROPOSITION 4.7 (Joint CLT of outlier eigenvalues). *Under Assumptions 2.1, 2.2 and 3.1, fix r and let $\xi_1 > \cdots > \xi_r$ be separated outliers of $\widetilde{\Sigma} = \Sigma + M$ with unit eigenvectors $\tilde{\psi}_1, \ldots, \tilde{\psi}_r$. Let $\boldsymbol{\lambda} = (\lambda_1, \ldots, \lambda_r)^\top$ be the r outlier sample eigenvalues of $Q = YY^\top/N$, and write $\boldsymbol{\xi}^{\mathbf{S}} = (\xi_1^{\mathrm{S}}, \ldots, \xi_r^{\mathrm{S}})^\top$ and θ for the outlier map with derivative $\theta_k' = \theta'(\xi_k^{\mathrm{S}})$. Assume a fixed outlier gap and the moment conditions stated above. Then we have $\sqrt{N}(\boldsymbol{\lambda} - \theta(\boldsymbol{\xi}^{\mathbf{S}})) \xrightarrow{d} \mathcal{N}_r(0, V_*)$, where the limiting covariance V_* admits the decomposition $V_* = \mathbb{E}[V^{\mathrm{cond}}] + N \, \nabla\theta(\boldsymbol{\xi}^{\mathbf{S}}) \Gamma^{(\mathrm{sig})} \nabla\theta(\boldsymbol{\xi}^{\mathbf{S}})^\top$. Here $\nabla\theta(\boldsymbol{\xi}^{\mathbf{S}}) = \mathrm{diag}(\theta_1', \ldots, \theta_r')$, and*

- *for the conditional noise block $V^{\mathrm{cond}} = (V_{kj}^{\mathrm{cond}})$, which is the conditional limiting covariance given S_{samp}, we have:*

$$V_{kj}^{\mathrm{cond}} = V_{kj}^{(G)} + \kappa_4 \, \theta_k' \theta_j' \, M_{2,2}(\Sigma^{1/2}\psi_k, \Sigma^{1/2}\psi_j) + 2 \, W_{kj} + 4 \, \theta_k' \theta_j' \, A_{kj} B_{kj},$$

with $A_{kj} = \psi_k^\top \Sigma \psi_j$, $B_{kj} = \psi_k^\top S_{\mathrm{samp}} S_{\mathrm{samp}}^\top \psi_j$,

$$V_{kk}^{(G)} = 2(\theta_k')^2 a_k^2 + 2\xi_k^{\mathrm{S}\,2} \theta_k' - 2\xi_k^{\mathrm{S}\,2}(\theta_k')^2, \quad W_{kj} = \kappa_3 \, \theta_k' \theta_j' \, A_{kj} B_{kj},$$

and $a_k = A_{kk}$.
- *for the signal-related variance block $N \, \nabla\theta(\boldsymbol{\xi}^{\mathbf{S}}) \Gamma^{(\mathrm{sig})} \nabla\theta(\boldsymbol{\xi}^{\mathbf{S}})^\top$, we have:*

$$\Gamma_{kj}^{(\mathrm{sig})} = \mathrm{Cov}\left(\tilde{\psi}_k^\top(\widehat{M} - M)\tilde{\psi}_k, \, \tilde{\psi}_j^\top(\widehat{M} - M)\tilde{\psi}_j\right)$$

$$= \frac{1}{N}\left\{\mathbb{E}[(\tilde{\psi}_k^\top S)^2(\tilde{\psi}_j^\top S)^2] - \mathbb{E}[(\tilde{\psi}_k^\top S)^2]\,\mathbb{E}[(\tilde{\psi}_j^\top S)^2]\right\} + o\left(\frac{1}{N}\right).$$

so that $\mathrm{Var}(\boldsymbol{\lambda}) = \frac{1}{N}\mathbb{E}[V^{\mathrm{cond}}] + \nabla\theta(\boldsymbol{\xi}^{\mathbf{S}}) \Gamma^{(\mathrm{sig})} \nabla\theta(\boldsymbol{\xi}^{\mathbf{S}})^\top + o\left(\frac{1}{N}\right)$.

4.4. *CLT of the nMSD estimator.* Recall that by Algorithm 2, we have

$$(27) \qquad \widehat{d}_j^2 = -\left(\frac{1}{p}\sum_{i=1}^p \frac{1}{\Sigma_{ii} - \widehat{\xi^{\mathrm{S}}}_j}\right)^{-1}, \qquad j = 1, \ldots, r.$$

Under the setting of Proposition 4.7, suppose $\theta'(\widehat{\xi^{\mathrm{S}}}_j) \neq 0$, we could use the relationship (14) to obtain a CLT for the estimator $\widehat{\xi^{\mathrm{S}}}_j$, and then use the relationship (27) to obtain a CLT for $\widehat{d}_j^2$ using Delta method. As a result, we can prove

$$\sqrt{N}\left(\widehat{d}^2 - d^2\right) \xrightarrow{d} \mathcal{N}(0, \Sigma_{d^2}),$$

where $\Sigma_{d^2} = \Gamma\, V_* \,\Gamma$, $d^2 = (d_1^2, \ldots, d_r^2)^\top$ and $\Gamma = \mathrm{diag}(\Gamma_1, \ldots, \Gamma_r)$ with

$$(28) \qquad \Gamma_j = \big[\mathrm{D}\big(\varphi \circ \theta^{-1}\big)(\xi^{\mathrm{S}})\big]_{jj} = \underbrace{\frac{s_2(\xi_j^{\mathrm{S}})}{p\, g(\xi_j^{\mathrm{S}})^2}}_{\varphi'(\xi_j^{\mathrm{S}})} \cdot \underbrace{\frac{1}{\theta'(\xi_j^{\mathrm{S}})}}_{(\theta^{-1})'(\theta(\xi_j^{\mathrm{S}}))} \,,$$

where D denotes the Jacobian matrix, and V_* is defined in subsection 4.3.2. To see this, note that for each j,

$$(29) \qquad \mathrm{Var}\big(\widehat{d}_j^2\big) = \Big(\frac{s_2(\xi_j^{\mathrm{S}})}{p\, g(\xi_j^{\mathrm{S}})^2}\Big)^2 \frac{\mathrm{Var}(\lambda_j)}{\big(\theta'(\xi_j^{\mathrm{S}})\big)^2} + o\Big(\frac{1}{N}\Big).$$

Let $s = \mathbf{1}^\top d^2$, and $\Pi = d^2/s \in \Delta^{r-1}$. With

$$(30) \qquad J_{kj}^\Pi = \frac{\partial \Pi_k}{\partial d_j^2} = \frac{\delta_{kj}\, s - d_k^2}{s^2},$$

and writing the componentwise maps $\xi = \theta^{-1}(\boldsymbol{\lambda})$ and $d^2 = \varphi(\xi)$, the Jacobians with respect to ξ are diagonal: $\mathrm{D}\theta^{-1}(\xi^{\mathrm{S}}) = \mathrm{diag}\big(1/\theta'(\xi_1^{\mathrm{S}}), \ldots, 1/\theta'(\xi_r^{\mathrm{S}})\big)$, and $\mathrm{D}\varphi(\xi^{\mathrm{S}}) = \mathrm{diag}\big(\varphi'(\xi_1^{\mathrm{S}}), \ldots, \varphi'(\xi_r^{\mathrm{S}})\big)$, with $\varphi'(s) = g'(s)/g(s)^2 = s_2(s)/(p\, g(s)^2)$ and therefore we have (28).

On the other hand, under the setting of Proposition 4.7, let $\widehat{\Pi} = \widehat{d}^2/(\mathbf{1}^\top \widehat{d}^2)$, $\Pi = d^2/(\mathbf{1}^\top d^2)$ and $s = \mathbf{1}^\top d^2 > 0$. Then we have

$$(31) \qquad \sqrt{N}\,\big(\widehat{\Pi} - \Pi\big) \xrightarrow{d} \mathcal{N}\big(0,\, \Sigma_\Pi\big),$$

on $T_\Pi \Delta^{r-1} := \{u \in \mathbb{R}^r : \mathbf{1}^\top u = 0\}$, where

$$(32) \qquad \Sigma_\Pi = J^\Pi\, \Gamma\, V_*\, \Gamma\, (J^\Pi)^\top, \qquad \Sigma_\Pi \mathbf{1} = \mathbf{0},\ \mathrm{rank}(\Sigma_\Pi) = r - 1.$$

With the above CLT for $\widehat{\Pi}$, we can then immediately obtain the CLT for the nMSD estimator.

4.5. Plug-in estimators.

We now explain how to turn the theoretical variance expressions into practical estimators. Throughout this subsection we suppress the dataset index k and work with a fixed sample covariance $Q = YY^\top/N$.

Let $(\lambda_j, \widehat{\psi}_j)$, $j = 1, \ldots, r$, be the outlier eigenpairs of Q, where $\widehat{\psi}_j$ is the jth sample eigenvector. In practice we use $\widehat{\psi}_j$ to approximate both the population outlier eigenvector $\widetilde{\psi}_j$ of $\widetilde{\Sigma} = \Sigma + M$ and the conditional outlier eigenvector ψ_j of $\Sigma + \widehat{M}$.

(1) Conditional (noise) block. Define the plug-in analogues of A_{kj}, B_{kj}, and $M_{2,2}$ by

$$\widehat{A}_{kj} := \widehat{\psi}_k^\top\, \widehat{\Sigma}\, \widehat{\psi}_j, \qquad \widehat{B}_{kj} := \widehat{\psi}_k^\top\, \widehat{M}\, \widehat{\psi}_j, \qquad \widehat{M}_{2,2}(k,j) := \sum_{a=1}^p \widehat{\psi}_{k,a}^2\, \widehat{\psi}_{j,a}^2\, \widehat{\Sigma}_{aa}^2,$$

where $\widehat{M}$ is the empirical signal covariance (for example, the rank-r fit) and $\widehat{\psi}_{k,a}$ denotes the ath coordinate of $\widehat{\psi}_k$.

To estimate the noise cumulants, we form residuals by projecting Y onto the orthogonal complement of the spike subspace spanned by $\widehat{\psi}_1, \ldots, \widehat{\psi}_r$:

$$\widehat{P} := \sum_{k=1}^r \widehat{\psi}_k \widehat{\psi}_k^\top, \qquad \widehat{R}_i := Y_i - \widehat{P} Y_i, \quad i = 1, \ldots, N,$$

and compute coordinatewise empirical moments

$$\widehat{m}_{2,a} = \frac{1}{N} \sum_{i=1}^N \widehat{R}_{a,i}^2, \quad \widehat{m}_{3,a} = \frac{1}{N} \sum_{i=1}^N \widehat{R}_{a,i}^3, \quad \widehat{m}_{4,a} = \frac{1}{N} \sum_{i=1}^N \widehat{R}_{a,i}^4.$$

The third and fourth standardized cumulants are then estimated by

$$\widehat{\kappa}_3 := \frac{1}{p} \sum_{a=1}^{p} \frac{\widehat{m}_{3,a}}{\widehat{m}_{2,a}^{3/2}}, \qquad \widehat{\kappa}_4 := \frac{1}{p} \sum_{a=1}^{p} \left(\frac{\widehat{m}_{4,a}}{\widehat{m}_{2,a}^2} - 3 \right).$$

Plugging these quantities into the conditional covariance formula yields

$$\widehat{V}_{kj}^{\mathrm{cond}} = \widehat{V}_{kj}^{(G)} + \widehat{\kappa}_4 \, \widehat{\theta}_k' \widehat{\theta}_j' \, \widehat{M}_{2,2}(k,j) + 2\widehat{W}_{kj} + 4\widehat{\theta}_k' \widehat{\theta}_j' \, \widehat{A}_{kj} \, \widehat{B}_{kj},$$

where

$$\widehat{V}_{kk}^{(G)} = 2(\widehat{\theta}_k')^2 \widehat{A}_{kk}^2 + 2\widehat{\xi}^{\mathrm{S}}{}_k^2 \, \widehat{\theta}_k' - 2\widehat{\xi}^{\mathrm{S}}{}_k^2 (\widehat{\theta}_k')^2, \qquad \widehat{W}_{kj} = \widehat{\kappa}_3 \, \widehat{\theta}_k' \widehat{\theta}_j' \, \widehat{A}_{kj} \, \widehat{B}_{kj}.$$

(2) Signal–sampling block. The signal–sampling covariance $\Gamma^{(\mathrm{sig})}$ was defined theoretically in Lemma 4.6 in terms of the population eigenvectors $\widetilde{\psi}_k$ and the true signal columns S_i. In practice we approximate $\widetilde{\psi}_k$ by $\widehat{\psi}_k$ and estimate the signal–sampling covariance via

$$\widehat{\Gamma}_{kj}^{(\mathrm{sig})} := \frac{2}{N} \, \widehat{B}_{kj}^2 + \frac{1}{N} \left(\widehat{\mathcal{K}}_Y - \widehat{\mathcal{K}}_\varepsilon \right) [\widehat{\psi}_k, \widehat{\psi}_k, \widehat{\psi}_j, \widehat{\psi}_j],$$

where $\widehat{\mathcal{K}}_Y$ and $\widehat{\mathcal{K}}_\varepsilon$ denote the empirical fourth–order cumulant tensors of Y and of the estimated noise, respectively.

(3) Variance of spikes. Combining the conditional and signal–sampling parts, the plug-in covariance matrix of the sample spikes is

$$\widehat{\mathrm{Var}}(\boldsymbol{\lambda}) = \frac{1}{N} \, \widehat{V}^{\mathrm{cond}} + \widehat{\nabla\theta} \, \widehat{\Gamma}^{(\mathrm{sig})} \, \widehat{\nabla\theta}^\top, \qquad \widehat{\nabla\theta} := \mathrm{diag}(\widehat{\theta}_1', \ldots, \widehat{\theta}_r'),$$

so in particular

$$\widehat{\mathrm{Var}}(\lambda_j) = \frac{1}{N} \, \widehat{V}_{jj}^{\mathrm{cond}} + \widehat{\theta}_j'^2 \, \widehat{\Gamma}_{jj}^{(\mathrm{sig})}.$$

Under symmetric Gaussian noise ($\kappa_3 = \kappa_4 = 0$) this simplifies to

$$\widehat{V}_{kj}^{\mathrm{cond}} = \widehat{V}_{kj}^{(G)} + 4 \, \widehat{\theta}_k' \widehat{\theta}_j' \, \widehat{A}_{kj} \, \widehat{B}_{kj},$$

and if moreover $\widehat{A}_{kj} \approx \widehat{B}_{kj} \approx 0$ for $k \neq j$, then $\widehat{V}^{\mathrm{cond}}$ is approximately diagonal.

(4) Variance of signal strengths and spectral profiles. Define the empirical counterparts of g and s_2 by replacing Σ with $\widehat{\Sigma}$ in their definitions:

$$\widehat{g}(s) := \frac{1}{p} \sum_{i=1}^{p} \frac{1}{\widehat{\sigma}_i - s}, \qquad \widehat{s}_2(s) := \sum_{i=1}^{p} \frac{1}{(\widehat{\sigma}_i - s)^2}.$$

The delta–method derivative for the mapping $\lambda_j \mapsto \widehat{d}_j^2$ is estimated by

$$\widehat{\Gamma}_j := \frac{\widehat{s}_2(\widehat{\xi}^{\mathrm{S}}{}_j)}{p \, \widehat{g}(\widehat{\xi}^{\mathrm{S}}{}_j)^2 \, \widehat{\theta}_j'}, \qquad \widehat{\Gamma} := \mathrm{diag}(\widehat{\Gamma}_1, \ldots, \widehat{\Gamma}_r).$$

Let $\widehat{V}_*$ denote the plug-in covariance of $\sqrt{N}(\boldsymbol{\lambda} - \theta(\widehat{\boldsymbol{\xi}^{\mathrm{S}}}))$ constructed above. Then the covariance matrices of $\widehat{d}^2$ and of the normalized profile $\widehat{\Pi}$ are estimated by

$$(33) \qquad \widehat{\Sigma}_{d^2} = \widehat{\Gamma} \, \widehat{V}_* \, \widehat{\Gamma}, \qquad \widehat{\Sigma}_\Pi = J^\Pi(\widehat{d}^2) \, \widehat{\Gamma} \, \widehat{V}_* \, \widehat{\Gamma} \, J^\Pi(\widehat{d}^2)^\top, \qquad \widehat{V}_\Pi = \frac{\widehat{\Sigma}_\Pi}{N},$$

and, under the same conditions as in (29)–(32), these plug-in estimators are consistent.

TABLE 1
Quantile comparison at the null ($r = 3$, $N = 1500$, ellipsoid-surface latent).

q	0.01	0.10	0.25	0.50	0.75	0.90	0.99
Emp. T_Π	0.019	0.223	0.569	1.280	2.601	4.688	9.423
χ_2^2	0.020	0.211	0.575	1.386	2.773	4.605	9.210
Diff (emp−th)	−0.001	0.012	−0.007	−0.106	−0.172	0.083	0.212

5. Simulation and real data applications.

5.1. *Comparison with existing methods using simulated data.* We evaluate the proposed methods under our manifold signal-plus-noise model (2), where X_i has i.i.d. $\mathcal{N}(0,1)$ entries. We let $\Sigma_i = \mathrm{diag}(\sigma_1^{(i)}, \ldots, \sigma_p^{(i)})$ be piecewise constant over four blocks (sizes $\approx p/3, p/6, p/6$, remainder) with levels $(3,4,5,6)$ for $i=1$ and $(2.5,3,6,4.5)$ for $i=2$. We fix $n = r = 3$, generate two independent samples of sizes $N_1 = N_2 = N$ (so $N_{\mathrm{eff}} = N/2$), set $p = 100$, and assess our methods by repeating each simulation setting n_{rep} times. For signal generation, we draw $V \in \mathbb{R}^{p \times r}$ with orthonormal columns by QR of a standard Gaussian matrix. For dataset i, fix semi–axes $D_i = (D_{i,1}, D_{i,2}, D_{i,3})$ and sample independent latent columns on the ellipsoid surface $x_j^{(i)} = \mathrm{diag}(D_i) v_j$, $v_j \sim \mathrm{Unif}(\mathbb{S}^{r-1})$. Set the deterministic signal $S_{\mathrm{samp},i} = \sqrt{r}\, V\, [x_1^{(i)}, \ldots, x_N^{(i)}]$, so that the population signal covariance equals $V \mathrm{diag}(D_i^2) V^\top$. The two datasets share V but have independent columns. For evaluation of our proposed test, at the null we take $D_1 = D_2 = (7,6,5)$; in power analysis we increase $D_{2,1}$ anisotropically.

We compare against Box's M [7], Energy distance [37], SMAI [32], MMD (Gaussian kernel) [22], Ball Divergence (BD) [35], Kernel Projected Wasserstein (KPW) [41], and a graph–based two–sample test (gTest) [11]. These act on observed expressions or low-dimensional embeddings, while our test compares trace-normalized signal–proportion vectors Π after explicit noise removal.

Experiment 1: Null calibration. Set $D_1 = D_2 = (7,6,5)$, $N_1 = N_2 = N = 1500$, and $n_{\mathrm{rep}} = 800$. Under the null hypothesis $H_0 : \Pi_1 = \Pi_2$, the statistic T_Π converges in distribution to χ_{r-1}^2 with $r - 1 = 2$ degrees of freedom. The empirical distribution of T_Π aligns closely with the χ_2^2 density (Figure C in Supplement). We also conduct a goodness-of-fit test (Figure C in Supplement); the resulting p-value is 0.867, providing no evidence against the χ_2^2 limit. The estimated size at level $\alpha = 0.05$ is 0.044, indicating mild conservativeness. Quantiles are close to those of χ_2^2 (Table 1); the largest discrepancy is ≈ 0.212 at the 99th percentile.

Experiment 2: Power vs. anisotropic separation. In this experiment, we illustrate the power of nMSD test. we fix $N_1 = N_2 = N = 3000$ and increase the first semi-axis of dataset 2 by a factor $c \in \{1.00, 1.05, 1.10, 1.20, 1.30, 1.50\}$: $D_2 = \sqrt{\mathrm{diag}(c,1,1)}\, D_1$. For each c we report separation $\|\Delta\Pi\|$, the noncentrality parameter λ of the asymptotic $\chi_{r-1}^2(\lambda)$, and empirical/theoretical power at level 0.05 ($n_{\mathrm{rep}} = 600$); see Table 2 and Supplementary Figure D. Power rises monotonically with $\|\Delta\Pi\|$; even for modest anisotropy ($c = 1.10$) the test attains power ≈ 0.53–0.55 and quickly approaches one once $c \geq 1.2$.

Scenario comparison with baselines. We compare the nMSD test with several related methods and summarize two representative scenarios using the same data generator.

In *Scenario A (noise only)*, the signal manifold is fixed across datasets while the noise level is scaled: $D_2 = D_1$, $\Sigma_2 = \alpha \Sigma_1$, $\alpha \in [1,2]$. In *Scenario B (signal reweighting)*, we anisotropically amplify the first signal axis (with scale removed) while keeping the noise

TABLE 2
Power and noncentrality ($r = 3$, $N_1 = N_2 = 3000$).

c	$\|\Delta\Pi\|$	λ (theory)	Power (theory)	Power (emp.)
1.00	0.00000	0.0000	0.0500	0.0417
1.05	0.01488	1.4371	0.1725	0.1833
1.10	0.02912	5.5051	0.5453	0.5233
1.20	0.05586	20.3010	0.9864	0.9833
1.30	0.08050	42.3648	1.0000	1.0000
1.50	0.12439	102.7337	1.0000	1.0000

profile fixed: $D_2 = \text{diag}(c, 1, 1) D_1$, $c \geq 1$, $\Sigma_2 = \Sigma_1$. All other aspects (dimension, rank, and sampling scheme) follow the main Monte Carlo design.

Figure 1 compares seven competitors—Box's M[7], Energy [37], SMAI [32], MMD [22], Ball Divergence (BD), Kernel Projected Wasserstein (KPW) [41], and a graph-based test (gTest) [11]—against the proposed nMSD test. The top row varies only the noise profile while keeping the signal manifold fixed; the bottom row increases the anisotropy of the first signal axis (c) while keeping the noise profile fixed. In the noise-only sweep (panels (a)–(b)), nMSD test remains well calibrated across the range: mean p-values stay near 0.5 and the rejection rate tracks the nominal size. By contrast, omnibus tests that target any covariance or distributional difference—Box's M, Energy, MMD, BD, KPW, and gTest—quickly move to very small mean p-values and near-unit rejection even under modest heteroskedasticity. SMAI exhibits noticeable size inflation that grows with the noise gap. When the signal proportion changes (panels (c)–(d)), nMSD test shows a steep power ramp: as c increases, mean p collapses and rejection approaches one by $c \approx 1.3$–1.4, matching its design to detect reallocation of variance across the top-r eigenvectors. BD and gTest also gain power but require somewhat larger separation; MMD and KPW improve more gradually. Box's M and Energy rise only slowly with c in this setting: their behavior is driven by omnibus sensitivity rather than the proportional-signal alternative. Together, these patterns separate hypotheses: nMSD test is stable under pure noise changes yet sharply responsive to signal-axis reallocation, whereas omnibus tests confound noise and signal and purely geometric alignment such as SMAI can miss proportional shifts.

The intended null equality of signal energy proportions in the top-r directions despite differing noise—is respected by nMSD test, which is insensitive to pure noise changes yet responsive to reallocation of signal variance. Baselines that test broader hypotheses conflate noise and signal and thus over-reject when only noise differs; purely geometric alignments tend to be conservative for axis reweighting.

5.2. *Analysis of human cardiac snRNA-seq data.* We analyzed the single-nucleus RNA-seq (snRNA-seq) arm of a public human myocardial infarction data [26](final processed dataset available on Zenodo, ID 7435911). After quality control, the dataset comprised 115,517 cell from 20 samples (16 donors) across two tissue states—control/remote and ischemic zone (IZ)—with 96,368 and 19,149 cells, respectively. UMI counts were library-size normalized (scale factor 10,000) and log-transformed (log1p). For downstream analyses, we restricted the feature set to the top 2,000 highly variable genes (HVGs) selected by a variance-stabilizing (vst) criterion for dimensionality reduction and clustering, while group-level comparisons were carried out at the donor×status level.

To enable cross-sample comparisons, we partitioned cells by *donor × tissue state* and, for each group, extracted the normalized expression matrix, yielding 17 data matrices. Each matrix has 2,000 genes by N_k cells (1,241–14,370 cells per matrix). Entries represent log-normalized expression derived from UMI counts; rows are HVGs and columns are cells.
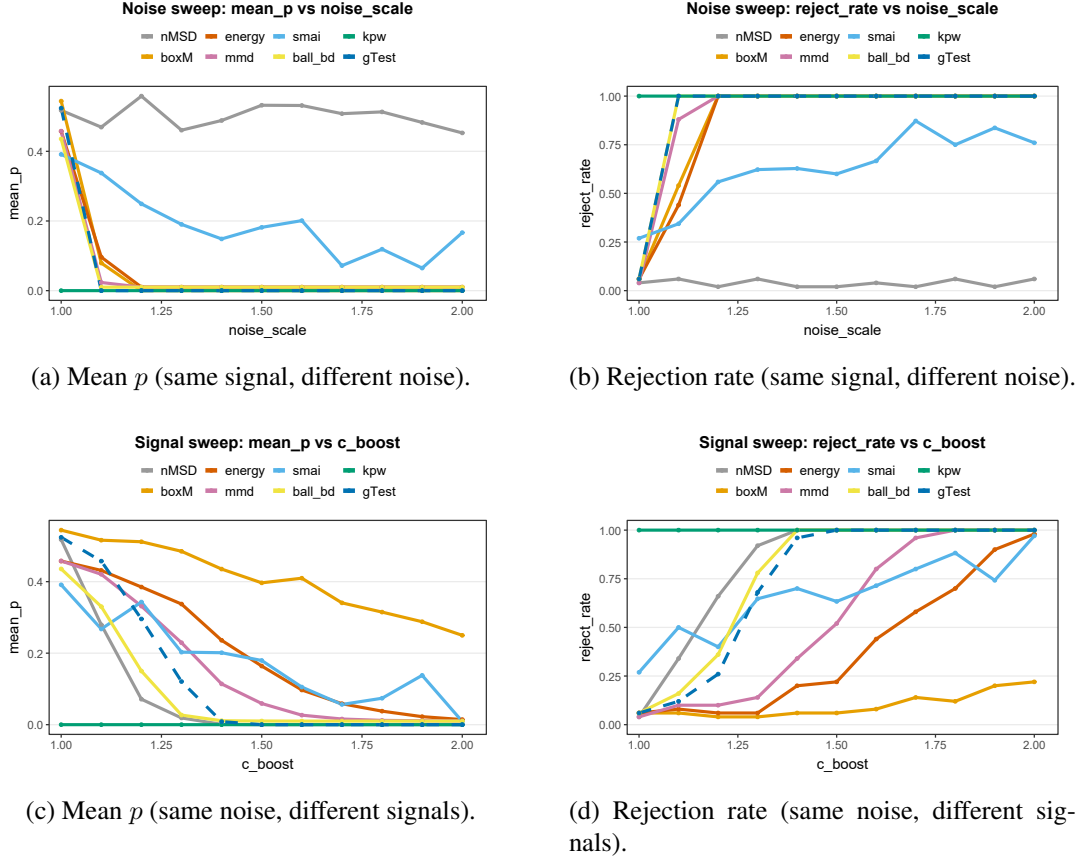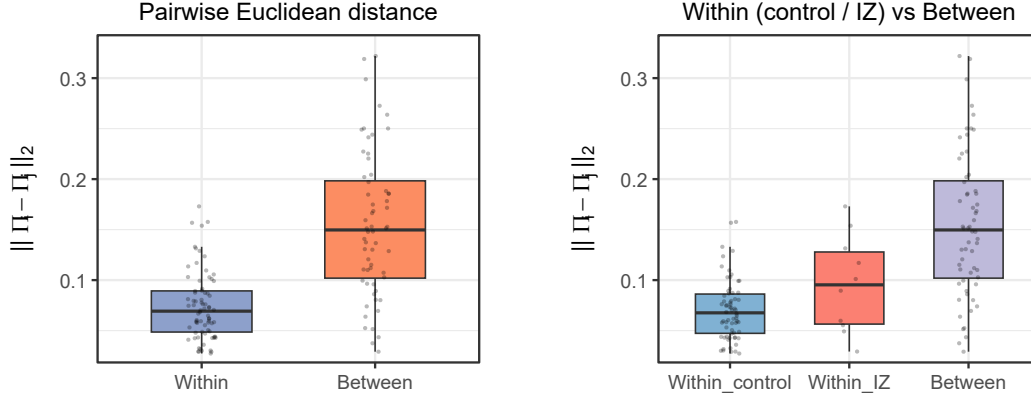
Noise sweep: mean_p vs noise_scale

nMSD — energy — smai — kpw
boxM — mmd — ball_bd — gTest

Noise sweep: reject_rate vs noise_scale

nMSD — energy — smai — kpw
boxM — mmd — ball_bd — gTest

(a) Mean p (same signal, different noise).

(b) Rejection rate (same signal, different noise).

Signal sweep: mean_p vs c_boost

nMSD — energy — smai — kpw
boxM — mmd — ball_bd — gTest

Signal sweep: reject_rate vs c_boost

nMSD — energy — smai — kpw
boxM — mmd — ball_bd — gTest

(c) Mean p (same noise, different signals).

(d) Rejection rate (same noise, different signals).

Fig 1: **Simulation summary across methods.** (a–b) Equal signal with different noise: mean p and rejection rate. (c–d) Equal noise with different signals: mean p and rejection rate.

Cell-level annotations (donor, state, cell type) were used only to define the donor × state splits.

For each matrix Y_k we estimated a diagonal, piecewise-constant noise covariance $\widehat{\Sigma}$ via factor analysis with one-dimensional segmentation and then applied Algorithm 2 to recover the top-r signal strengths $\widehat{d}^2 = (\widehat{d}_1^2, \ldots, \widehat{d}_r^2)$ by inverting the outlier map under the fitted noise model. We formed the trace-normalized principal-variance vector and computed pairwise nMSD distances $\mathrm{dist}_{ij} = \left\| \widehat{\Pi}_{r,i} - \widehat{\Pi}_{r,j} \right\|_2$ across all donors. Distances were grouped into *Within_control*, *Within_IZ*, and *Between* (IZ vs. control) according to the states of the two donors. We expect the *Between* distances to be significantly larger than *Within* distances because the samples from the same state should share a similar underlying structure.
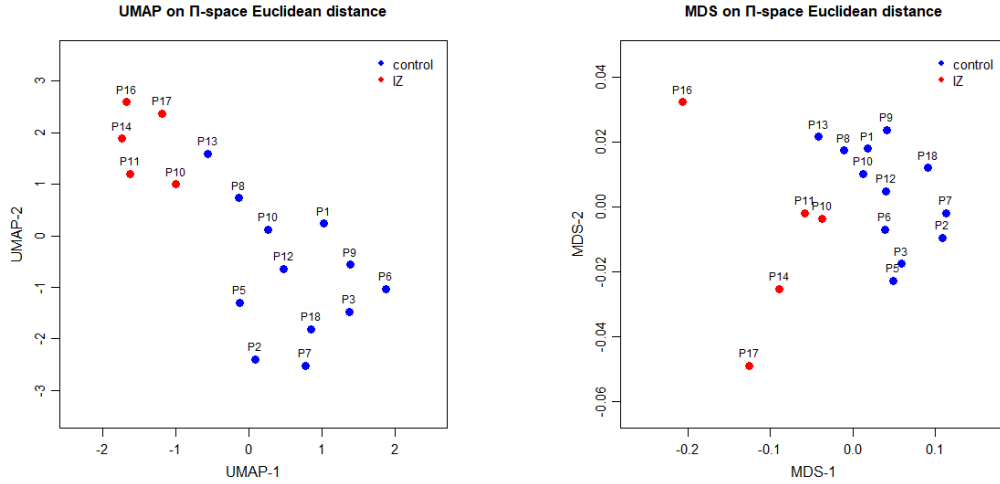
Figure 2 summarizes the resulting distributions. *Between* distances are markedly larger than *Within* distances, indicating that IZ and control exhibit distinct allocations of variance onto their leading signal directions once heterogeneous noise has been accounted for and overall scale normalized. Moreover, *Within_IZ* distances exceed *Within_control*, suggesting greater inter-donor heterogeneity of the IZ samples. To visualize these relationships at the donor level, we embedded the donor × donor distance matrix using UMAP and classical MDS (Figure 3). Donors separate cleanly by condition in both views, showing that the top-r principal-variance patterns encoded by $\widehat{\Pi}_r$ carry condition-specific structure. All donors were processed under an identical pipeline (same HVGs and a fixed working rank r across matrices). Because distances are computed from trace-normalized principal variances after explicit

(a) Between vs. within spectral distances. Each point is $\|\widehat{\Pi}_{r,i} - \widehat{\Pi}_{r,j}\|_2$ for a donor pair.

(b) Within-group dispersion by condition.

Fig 2: **Pairwise $\widehat{\Pi}_r$–based distances.** Panel a compares donor-pair distances between and within conditions; panel b decomposes within-condition dispersion.

(a) UMAP on the spectral-distance matrix.

(b) Classical MDS on the spectral-distance matrix.

Fig 3: **Low-dimensional embeddings from $\widehat{\Pi}_r$–based distances.** Donors separate by condition in both views, indicating that top-r principal-variance patterns are condition-informative.

noise estimation, observed differences should be interpreted as genuine biological variation along the leading directions, rather than artifacts of scaling or noise anisotropy.

SUPPLEMENTARY MATERIAL

Supplement to "Statistical Inference of Manifold Similarity and Alignability across Noisy High-Dimensional Datasets"
The supplementary material [13] contains technical proofs of the main theorems, some examples and further details of the assumed block structure of noise.

REFERENCES

[1] BAI, Z. and SILVERSTEIN, J. W. (2010). *Spectral analysis of large dimensional random matrices* **20**. Springer.

[2] BALASUBRAMANIAN, K., LI, T. and YUAN, M. (2021). On the Optimality of Kernel-Embedding Based Goodness-of-Fit Tests. *Journal of Machine Learning Research* **22** 1–45.

[3] BAO, Z., DING, X. and WANG, K. (2021). SINGULAR VECTOR AND SINGULAR SUBSPACE DIS-TRIBUTION FOR THE MATRIX DENOISING MODEL. *The Annals of Statistics* **49** 370–392.

[4] BAO, Z., HU, J., PAN, G. and ZHOU, W. (2019). Canonical correlation coefficients of high-dimensional Gaussian vectors: Finite rank case. *The Annals of Statistics* **47** 612–640.

[5] BARINGHAUS, L. and FRANZ, C. (2004). On a new multivariate two-sample test. *Journal of Multivariate Analysis* **88** 190–206.

[6] BENGIO, Y., COURVILLE, A. and VINCENT, P. (2013). Representation learning: A review and new per-spectives. *IEEE transactions on pattern analysis and machine intelligence* **35** 1798–1828.

[7] BOX, G. E. P. (1949). A General Distribution Theory for a Class of Likelihood Criteria. *Biometrika* **36** 317–346.

[8] BOYSEN, L., KEMPE, A., LIEBSCHER, V., MUNK, A. and WITTICH, O. (2009). Consistencies and rates of convergence of jump-penalized least squares estimators. *The Annals of Statistics* **37**. https://doi.org/10.1214/07-aos558

[9] CAI, T., LIU, W. and XIA, Y. (2013). Two-sample covariance matrix testing and support recovery in high-dimensional and sparse settings. *Journal of the American Statistical Association* **108** 265–277.

[10] CAO, Y., YANG, S., LI, C., XIANG, H., QI, L., LIU, B., LI, R. and LIU, M. (2025). TAD-Bench: A Comprehensive Benchmark for Embedding-Based Text Anomaly Detection.

[11] CHEN, H., CHEN, X. and SU, Y. (2016). A weighted edge-count two-sample test for multivariate and object data. *arXiv preprint arXiv:1604.06515*.

[12] CHEN, H. and FRIEDMAN, J. H. (2016). A new graph-based two-sample test for multivariate and object data. *Journal of the American statistical association*.

[13] CHEN, H. and MA, R. (2025). Supplement to "Statistical Inference of Manifold Similarity and Alignability across Noisy High-Dimensional Datasets".

[14] CHU, L. and DAI, X. (2024). Manifold energy two-sample test. *Electronic Journal of Statistics* **18** 145–166. https://doi.org/10.1214/23-EJS2203

[15] DING, X. and MA, R. (2023). Learning Low-Dimensional Nonlinear Structures from High-Dimensional Noisy Data: An Integral Operator Approach. *The Annals of Statistics* **51** 1744–1769. https://doi.org/10.1214/23-AOS2306

[16] DING, X. and MA, R. (2025). Kernel spectral joint embeddings for high-dimensional noisy datasets using duo-landmark integral operators. *Journal of the American Statistical Association* 1–28.

[17] DING, X. and WU, H.-T. (2024). How do kernel-based sensor fusion algorithms behave under high-dimensional noise? *Information and Inference: A Journal of the IMA* **13** iaad051.

[18] DING, X. and YANG, F. (2021). Spiked separable covariance matrices and principal components. *The Annals of Statistics* **49** 1113–1138. https://doi.org/10.1214/20-AOS1995

[19] DONOHO, D. and GAVISH, M. (2014). Minimax risk of matrix denoising by singular value thresholding. *The Annals of Statistics* **42**.

[20] ERDŐS, L. and YAU, H.-T. (2017). *A dynamical approach to random matrix theory* **28**. American Mathematical Soc.

[21] FEFFERMAN, C., MITTER, S. and NARAYANAN, H. (2016). Testing the manifold hypothesis. *Journal of the American Mathematical Society* **29** 983–1049.

[22] GRETTON, A., BORGWARDT, K. M., RASCH, M. J., SCHÖLKOPF, B. and SMOLA, A. J. (2012). A Kernel Two-Sample Test. *Journal of Machine Learning Research* **13** 723–773.

[23] GRETTON, A., FUKUMIZU, K., HARCHAOUI, Z. and SRIPERUMBUDUR, B. K. (2009). A Fast, Consistent Kernel Two-Sample Test. In *Advances in Neural Information Processing Systems*.

[24] JANSSENS, K. G. F., RAABE, D., KOZESCHNIK, E., MIODOWNIK, M. A. and NESTLER, B., eds. (2007). *Computational Materials Engineering: An Introduction to Microstructure Evolution*. Academic Press, Burlington, MA.

[25] JIANG, D. (2023). A Universal Test on Spikes in a High-Dimensional Generalized Spiked Model and Its Applications. *Statistica Sinica* **33** 1749–1770. https://doi.org/10.5705/ss.202021.0346

[26] JOODAKI, M., SHAIGAN, M., PARRA, V., BÜLOW, R. D., KUPPE, C., HÖLSCHER, D. L., CHENG, M., NAGAI, J. S., GOEDERTIER, M., BOUTELDJA, N., TESAR, V., BARRATT, J., ROBERTS, I. S. D., COPPO, R., KRAMANN, R., BOOR, P. and COSTA, I. G. (2024). Detection of PatIent-Level distances from single cell genomics and pathomics data with Optimal Transport (PILOT). *Molecular Systems Biology* **20** 57–74. Epub 2023 Dec 19. https://doi.org/10.1038/s44320-023-00003-8

[27] LI, J. (2018). Asymptotic normality of interpoint distances for high-dimensional data with applications to the two-sample problem. *Biometrika* **105** 529–546. https://doi.org/10.1093/biomet/asy020

[28] LI, W., WANG, Q. and YAO, J. (2023). Eigenvalue distribution of a high-dimensional distance covariance matrix with application. *Statistica Sinica* **33** 149–168.

[29] LIN, Z., PAN, G., ZHAO, P. and ZHOU, J. (2024). Asymptotic Distribution of Spiked Eigenvalues in the Large Signal-Plus-Noise Model. *arXiv preprint arXiv:2401.11672*.

[30] LIU, W. (2013). GAUSSIAN GRAPHICAL MODEL ESTIMATION WITH FALSE DISCOVERY RATE CONTROL. *The Annals of Statistics* **41** 2948–2978.

[31] LUO, Y.-W., REN, C.-X., DAI, D.-Q. and YAN, H. (2020). Unsupervised domain adaptation via discriminative manifold propagation. *IEEE transactions on pattern analysis and machine intelligence* **44** 1653–1669.

[32] MA, R., SUN, E. D., DONOHO, D. and ZOU, J. (2024). Principled and interpretable alignability testing and integration of single-cell data. *Proc Natl Acad Sci U S A* **121** e2313719121. Epub 2024 Feb 28. https://doi.org/10.1073/pnas.2313719121

[33] MEILĂ, M. and ZHANG, H. (2024). Manifold learning: What, how, and why. *Annual Review of Statistics and Its Application* **11** 393–417.

[34] MESTRE, X., VALLET, P., LOUBATON, P. and HACHEM, W. (2011). Asymptotic analysis of a consistent subspace estimator for observations of increasing dimension. In *2011 IEEE Statistical Signal Processing Workshop (SSP)* 677–680. IEEE.

[35] PAN, W., TIAN, Y., WANG, X. and ZHANG, H. (2018). Ball Divergence: Nonparametric Two Sample Test. *The Annals of Statistics* **46** 1109–1137. https://doi.org/10.1214/17-AOS1579

[36] PAUL, D. (2007). Asymptotics of sample eigenstructure for a large dimensional spiked covariance model. *Statistica Sinica* 1617–1642.

[37] RIZZO, M. L. and SZÉKELY, G. J. (2016). Energy distance. *Wiley Interdisciplinary Reviews: Computational Statistics* **8** 27–38. https://doi.org/10.1002/wics.1375

[38] SARKAR, S. and GHOSH, A. K. (2018). On some high-dimensional two-sample tests based on averages of inter-point distances. *Stat.* https://doi.org/10.1002/sta4.187

[39] SMALE, S. and ZHOU, D.-X. (2009). Geometry on Probability Spaces. *Constructive Approximation* **30** 311–323. https://doi.org/10.1007/s00365-009-9070-2

[40] SZÉKELY, G. J. and RIZZO, M. L. (2004). Testing for equal distributions in high dimension. Preprint.

[41] WANG, J., GAO, R. and XIE, Y. (2022). Two-Sample Test with Kernel Projected Wasserstein Distance. In *Proceedings of the 25th International Conference on Artificial Intelligence and Statistics (AISTATS)*. *Proceedings of Machine Learning Research* **151** 8003–8021. PMLR.

[42] WEINMANN, A., STORATH, M. and DEMARET, L. (2015). The L1-Potts Functional for Robust Jump-Sparse Reconstruction. *SIAM Journal on Numerical Analysis* **53** 644-673. https://doi.org/10.1137/120896256

[43] WU, H.-T. and WU, N. (2018). THINK GLOBALLY, FIT LOCALLY UNDER THE MANIFOLD SETUP: ASYMPTOTIC ANALYSIS OF LOCALLY LINEAR EMBEDDING. *The Annals of Statistics* **46** 3805–3837.

[44] XIA, Y., CAI, T. and CAI, T. T. (2015). Testing differential networks with applications to the detection of gene-gene interactions. *Biometrika* **102** 247–266.

[45] XIA, Y., CAI, T. and CAI, T. T. (2018). Multiple testing of submatrices of a precision matrix with applications to identification of between pathway interactions. *Journal of the American Statistical Association* **113** 328–339.

[46] YAN, Y., CHEN, Y. and FAN, J. (2024). Inference for heteroskedastic PCA with missing data. *The Annals of Statistics* **52** 729–756.

[47] YANG, F. (2022). Limiting distribution of the sample canonical correlation coefficients of high-dimensional random vectors. *Electronic Journal of Probability* **27** 1–71.